Tectonics®

RESEARCH ARTICLE
10.1029/2025TC008952

Rupture and Relamination of Continental Lithosphere in a Subduction System (Variscan Orogeny, SW Iberia)

Rubén Díez Fernández[1], Diana Moreno-Martín[2], Alejandro Díez Montes[1], Esther Rojo-Pérez[3], Irene Novo-Fernández[4], Luis Miguel Martín Parra[1], Jerónimo Matas[1], and Francisco J. Rubio Pascual[1]

[1]Departamento de Geología y Subsuelo, CN-IGME-CSIC, Madrid, Spain, [2]Departamento de Mineralogía y Petrología, Universidad Complutense, Madrid, Spain, [3]Geochronology section, Senckenberg Naturhistorische Sammlungen Dresden, Dresden, Germany, [4]Departamento de Mineralogía y Petrología, Universidad de Granada (UGR), Granada, Spain

Key Points:

- Early Variscan high-P rock exhumation in SW Iberia was assisted by an intra-subduction zone lithosphere-scale thrust (Llera thrust)
- The Llera thrust was bent into large recumbent folds formed during synthetic and antithetic shearing relative to subduction polarity
- Thrust-assisted exhumation and folding are framed into a process of relamination of continental high-P rocks before the Variscan collision

Supporting Information:

Supporting Information may be found in the online version of this article.

Correspondence to:

R. Díez Fernández,
r.diez@igme.es

Citation:

Díez Fernández, R., Moreno-Martín, D., Díez Montes, A., Rojo-Pérez, E., Novo-Fernández, I., Martín Parra, L. M., et al. (2025). Rupture and relamination of continental lithosphere in a subduction system (Variscan Orogeny, SW Iberia). *Tectonics*, *44*, e2025TC008952. https://doi.org/10.1029/2025TC008952

Received 9 APR 2025
Accepted 25 JUN 2025

Author Contributions:

Conceptualization: Rubén Díez Fernández
Data curation: Rubén Díez Fernández, Alejandro Díez Montes
Formal analysis: Rubén Díez Fernández, Diana Moreno-Martín, Alejandro Díez Montes, Esther Rojo-Pérez, Irene Novo-Fernández, Luis Miguel Martín Parra, Jerónimo Matas, Francisco J. Rubio Pascual
Funding acquisition: Rubén Díez Fernández, Francisco J. Rubio Pascual
Investigation: Rubén Díez Fernández, Diana Moreno-Martín, Esther Rojo-Pérez, Irene Novo-Fernández, Luis

Abstract Relamination is closely connected to subduction zones. Despite the numerous high-P metamorphic belts recognized on Earth, relamination remains a poorly documented process. We present a continental subduction zone where the exhuming high-P rocks became a relaminant under the upper plate. This study focuses on the Variscan Orogeny (SW Iberia) and is based on geological mapping and structural, metamorphic, and geochronological analysis. A lithospheric-scale thrust within the subduction zone conducted the early exhumation of the high-P rocks. This thrust brought deeper sections of the slab onto shallower ones. The exhumation assisted by this thrust proceeded up to the base of the upper plate, which locked the exhumation path of the high-P rocks through the subduction zone. At this point, the high-P rocks became a relaminant that moved under the upper plate and away from the subduction zone. A combination of synthetic and anti-thetic shearing relative to the subduction polarity conducted relamination. The shear zones formed at this point coexisted with the narrowing of the subduction system upon a progressive arrival of a more buoyant lithosphere to the subduction zone. The combination of both processes resulted in large-scale recumbent folds, which affected the early thrusts and contributed to the relamination process by facilitating subhorizontal flow during fold amplification. The ensuing collisional stage affected the whole subduction system (lower and upper plate, collectively) and led to an out-of-sequence thrust system that duplicated the suture zone defined by the high-P rocks.

1. Introduction

Recognizing the mechanism(s) by which high-P rocks are exhumed after subduction has received much attention from field-based geologists and modelers (e.g., Gerya, 2022; Hacker et al., 2013). A simple way to classify the plethora of processes and mechanisms invoked is to consider whether they operate within or outside the subduction channel. Some popular mechanisms that occur within the channel are the forced return flow of low-viscosity material giving way to tectonic mélanges (Gerya et al., 2002; Platt, 1993; Wakabayashi, 2015) and the rising of large (internally coherent) buoyant rock bodies along the upper-lower plate interface (Beaumont et al., 2009; Burov et al., 2001; Chemenda et al., 1995; Gerya et al., 2002, 2008; Warren et al., 2008), which may be promoted by the insertion of strong (cold) material into the subduction system (Grujic et al., 2011; Kellett et al., 2010; Warren et al., 2008, 2011). Among the mechanisms that can operate outside the subduction channel, we may have erosion, eduction (Andersen et al., 1991; Duretz et al., 2012), the development of trans-mantle diapirs (Castro et al., 2013; Little et al., 2011; Schulmann et al., 2014) or the extensional orogenic collapse (Arango et al., 2013; Díez Fernández et al., 2012; Jolivet & Brun, 2010; Vanderhaeghe, 2012; Vanderhaeghe et al., 2020). Moreover, subduction, and particularly continental subduction, heralds continental collision, which can contribute to further rock exhumation but come along with superimposed deformation and complicate the recognition of the subduction-related record (e.g., Díez Fernández et al., 2024). These mechanisms represent end-members because they may interfere with one another (Franek et al., 2011; Franke & Stein, 2000; Guilmette et al., 2011; Kali et al., 2010; Konopasek & Schulmann, 2005; Warren et al., 2011).

Numerical and analog modeling have contributed to understanding high-P rock exhumation (e.g., Beaumont et al., 2009; Burov et al., 2014; Chemenda et al., 1995; Gerya, 2022). Some of these models indicate a quite challenging evolution to decipher from the perspective of a field-based study. The sequence of deformation events that can be observed in the simulations includes re-folding, folds affecting shear zones, shear zones cutting folds, contractional and extensional shear zones operating simultaneously or diachronically, and any combination of the

10.1029/2025TC008952

Miguel Martín Parra, Jerónimo Matas, Francisco J. Rubio Pascual
Methodology: Rubén Díez Fernández, Diana Moreno-Martín, Alejandro Díez Montes, Esther Rojo-Pérez, Irene Novo-Fernández
Project administration: Rubén Díez Fernández, Francisco J. Rubio Pascual
Resources: Rubén Díez Fernández
Software: Rubén Díez Fernández
Supervision: Rubén Díez Fernández
Validation: Rubén Díez Fernández, Diana Moreno-Martín, Alejandro Díez Montes, Esther Rojo-Pérez
Visualization: Rubén Díez Fernández
Writing – original draft: Rubén Díez Fernández, Diana Moreno-Martín, Alejandro Díez Montes, Esther Rojo-Pérez, Francisco J. Rubio Pascual
Writing – review & editing: Rubén Díez Fernández, Diana Moreno-Martín, Alejandro Díez Montes, Esther Rojo-Pérez, Irene Novo-Fernández, Luis Miguel Martín Parra, Jerónimo Matas, Francisco J. Rubio Pascual

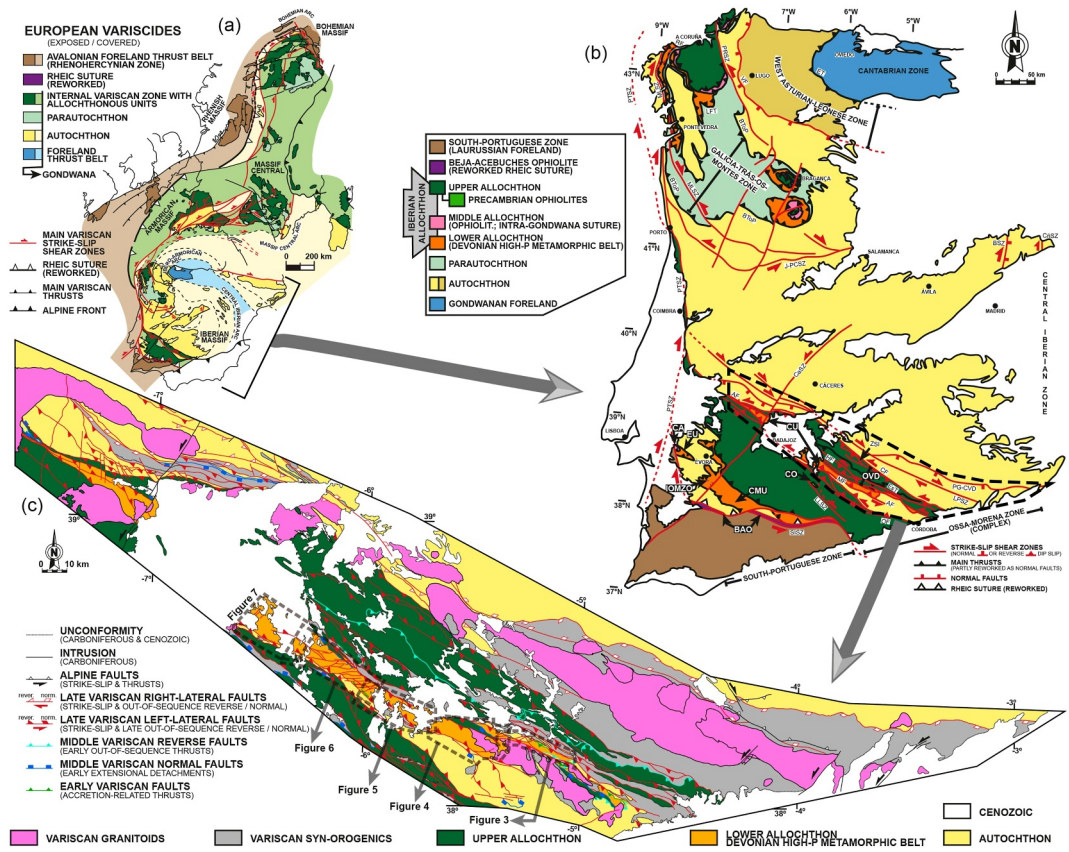

Figure 1. Location of the study area in the Variscan orogen (Díez Fernández & Arenas, 2015), including (a) map of the main Variscan terranes in Europe, (b) in the Iberian Massif and (c) in the SW part of the Iberian Massif. The boundaries of the maps presented in Figures 3–7 are indicated. Abbreviations: AF—Azuaga Fault; BToIP—Basal Thrust of the Parautochthon; BAO—Beja–Acebuches Ophiolite; BSZ—Berzosa Shear Zone; CA—Carvalhal Amphibolites; CaF—Cañaveral Shear Zone; CñF—Cañamares Shear Zone; CF—Canaleja Fault; CMU—Cubito–Moura Unit; CO—Calzadilla Ophiolite; CU—Central Unit; EsT—Espiel Thrust; EU—Escoural Unit; ET—Espina Thrust; HF— Hornachos Fault; IOMZO —Internal Ossa-Morena Zone Ophiolites; J–PCSZ—Juzbado-Penalva do Castelo Shear Zone; LFT—Lalín-Forcarei Thrust; LPSZ—Los Pedroches Shear Zone; LLSZ—Llanos Shear Zone; MLSZ—Malpica–Lamego Shear Zone; MF—Matachel Fault; OF—Onza Fault; OVD—Obejo–Valsequillo Domain; PG–CVD—Puente Génave–Castelo de Vide Detachment; PRSZ— Palas de Rei Shear Zone; PTSZ—Porto–Tomar Shear Zone; RF—Riás Fault; SISZ —South Iberian Shear Zone; VF—Viveiro Fault; ZSI—Zalamea de la Serena Imbricates.

previous examples. In reality, the metamorphic belts containing high-P rocks are structurally complex and are usually affected by polyphase deformation (e.g., Díez Fernández et al., 2011; Faure et al., 2003; Jolivet et al., 2003; Schulmann et al., 2014; Warren, 2013). Additionally, complexity can be derived from deformation within and/or outside the subduction channel, for instance, during a collisional stage (e.g., Díez Fernández et al., 2024). The simplest view of a subduction zone would consider it as a large-scale shear zone located between the descending and overriding plate with coherent kinematics. In shear zones, rocks can accumulate contrasted deformation as shearing progresses (e.g., Fossen & Cavalcante, 2017). This should also be true for high-P rocks in nature. However, subduction zones are lithosphere-scale structures, so the sequence of deformational processes should have an imprint on a large scale (tens of km). Accordingly, mapping geological structures affecting high-P rocks at the regional scale emerges as a critical tool to ground truth the exhumation mechanism(s) operating in a continental subduction zone.

The number of variables that shape the exhumation of high-P rocks prevents us from applying a reductionist solution to all cases. This leads us to a case-by-case and holistic approach that must deal with the specifics of each case. In this paper, we discuss the mechanisms by which a high-P metamorphic belt was exhumed and exposed in the core of the Iberian Massif (southern Europe; Figure 1). The main focus is on deciphering the macrostructural imprint related to the early record of high-P rocks exhumation and the lithosphere-scale processes and

mechanisms that contributed to it. To this purpose, we have recognized the geometry and relative timing of the structures that affect the high-P metamorphic belt and its surrounding rocks. Our results document the development of a lithospheric-scale thrust within the subduction zone and the relamination (tectonic underplating) of its hanging wall block to the base of the upper plate crust. The ensuing deformation affects the whole subduction system (lower and upper plate, collectively) and is framed into the following collisional stage. In the literature, few cases of a continental lithosphere relamination process have been documented through geological studies (e.g., Johnston et al., 2007; Schulmann et al., 2014). Here, we present structural, metamorphic, and geochronological evidence of each step of such process.

2. Geological Setting: Pieces of the Devonian Continental Subduction Complex in SW Iberia

The study case is located in the SW section of the Iberian Massif (Figure 1), which resulted from the collision of Laurussia, Gondwana, and their peripheral terranes during the Variscan Orogeny (Díez Fernández et al., 2016; Kroner & Romer, 2013; Martínez Catalán et al., 2021; Matte, 2001; Schulmann et al., 2014). This late Paleozoic orogen was formed after the consumption of several oceanic basins located between Gondwana-derived terranes and Laurussia (e.g., Martínez Catalán et al., 2021; Simancas et al., 2009). The SW Iberian Massif contains two types of suture zones, i.e., one that separates Gondwana-derived terranes (i.e., intra-Gondwana suture) and another one separating the latter from terranes with Laurussian affinity (Figure 1). The intra-Gondwana suture zone contains Devonian high-P metamorphic rocks formed during continental subduction (Abalos et al., 1991b; Arenas et al., 2021; López Sánchez-Vizcaíno et al., 2003; Novo-Fernández et al., 2021; Pereira, Apraiz, et al., 2010) and are the focus of our work. Relatively continuous exposure of this Devonian suture zone occurs in SW Iberia, along a metamorphic belt that strikes NW-SE (Figure 1; Abalos, 1990; Azor, 1994). This high-P metamorphic belt is surrounded by mid-to low-P metamorphic rock ensembles and has been correlated with other Devonian high-P metamorphic belts occurring throughout the Iberian Massif (Figure 1; Díez Fernández & Arenas, 2015).

The rock sequences primarily below the aforementioned Devonian suture zone show Gondwanan affinity (Fuenlabrada et al., 2021; Solís-Alulima et al., 2022) and have been referred to as Autochthon (Figure 1; Díez Fernández & Arenas, 2015, 2016). The high-P metamorphic belt is bounded by strike-slip faults that belong to a major late Variscan system formed under sinistral transpression (Figure 1c; Coimbra-Badajoz-Córdoba shear zone; Abalos & Eguiluz, 1991; Azor et al., 1994; Burg et al., 1981; Díez Fernández, Fernández, et al., 2021, Díez Fernández, Fernández, et al., 2022; Pereira, Silva, et al., 2010). These faults cut across the internal structure of the high-P metamorphic belt, which is dominated by a mylonitic foliation formed after Devonian high-P metamorphism (Abati et al., 2018; Azor et al., 1994; Pereira, Apraiz, et al., 2010). The rocks primarily on top of the high-P metamorphic belt are referred to as Upper Allochthon (Figures 1b and 1c). These rocks exhibit a polyorogenic tectonometamorphic evolution related first to the Cadomian orogeny (Ediacaran to Cambrian; Arenas et al., 2018; Díez Fernández, Arenas, et al., 2022; Díez Fernández et al., 2019; Eguíluz et al., 2000; Quesada, 1990; Rojo-Pérez et al., 2022), and after to Variscan folds and faults (Late Devonian to Carboniferous; Díez Fernández, Matas, et al., 2021; Eguíluz et al., 2000; Expósito et al., 2002, 2003; Martínez Poyatos et al., 2001; Moreno-Martín et al., 2025, 2023).

The high-P metamorphic belt is surrounded (initially covered) by syn-orogenic strata ranging in age from the Tournaisian to the Gzhelian (Azor, 1994; Martínez Poyatos, 2002; Matas, Martín Parra, Roldán, & Martín-Serrano, 2015). The older Carboniferous series were deposited in marine environments (e.g., Armendariz et al., 2008), while the younger ones were deposited in intramountainous settings (Wagner, 2004). Most Carboniferous series are affected by Variscan deformation and metamorphism, while some include Mississippian, basic-intermediate volcanic rocks that are also deformed, metamorphosed and juxtaposed against the high-P metamorphic rocks by late Variscan faults (Díez Fernández, Fernández, et al., 2021; Sarrionandia et al., 2023).

In this work, the description of the major structures will be based on a nomenclature aimed at deciphering the tectonics of a Variscan subduction system. Since later deformation heavily distorted this system, some names refer to its primary, Late Devonian to earliest Early Carboniferous architecture.

2.1. Upper Plate (Upper Allochthon)

The term upper plate will be applied to the rocks that occupied an upper structural position (on top of a mantle wedge) while Devonian intra-Gondwana subduction occurred. These rocks are usually deformed under low-P and low-T metamorphic conditions during the Variscan orogenesis (greenschist facies; chlorite zone, some sections reached the biotite zone).

The upper plate ensemble includes Ediacaran metagreywackes, phyllites, schists, and black quartzites that belong to the Serie Negra Group (Gp.), which is divided into the Montemolín (older) and Tentudía formations (Eguíluz, 1987). It is unconformably covered by Ediacaran-Cambrian phyllites and meta-volcanic rocks (Malcocinado Fm.), which are also unconformably covered by Cambrian strata, including meta-sandstones, phyllites, slates, and marble (Torreárboles and Zafra formations) (e.g., Díez Fernández et al., 2019; Eguíluz, 1987).

2.2. High-P Metamorphic Belt (Lower Allochthon)

The term high-P metamorphic belt refers to the rocks that experienced early Variscan (late Devonian) deformation under a high-P and low-to mid-T metamorphic conditions. These rocks are considered pieces of a continental slab that were exhumed after subduction.

The high-P metamorphic belt includes metasedimentary and metaigneous rocks, with protolith ages ranging between Ediacaran and Ordovician (Abalos, 1990; Abati et al., 2018; Azor, 1994; Gómez-Pugnaire et al., 2003; Ordóñez Casado, 1998). The high-P metamorphic belt can be divided into two main formations, namely the Montemolín and Atalaya formations. The Montemolín Fm. consists of schists, albite-bearing schists, garnet-bearing schists, paragneisses, migmatitic paragneisses (sample UC-3), meta-greywackes (sample UC-1), white quartzites, black quartzites, amphibolites (sample UC-12), (retro-)eclogites, felsic (sometimes augen) orthogneisses (sample UC-10) and mafic orthogneisses and mafic granulites. The Atalaya Fm. (Chacón, 1979) contains muscovite-rich mica-schists, garnet-bearing mica-schists (sample UC-4), (white to cream-colored) meta-sandstones, and felsic (sometimes augen) orthogneisses (samples UC-2 and 5).

The two main formations of the high-P metamorphic belt are separated by a discontinuous band of ultramafic rocks including serpentinites (after peridotites with a likely spinel facies orogenic lherzolite precursor) and other metamorphosed ultramafic rocks such as chlorite-talc schists, tremolite-talc-chlorite rocks and magnesio-hornblende chlorite rocks (see further descriptions provided by Ábalos et al., 2023; Chacón, 1979; Chacón & Velasco, 1981), referred to as the Ribera del Fresno-Llera ultramafics.

2.3. Autochthon

Autochthon refers to a group of rocks that experienced early Variscan deformation under mid-P and low-to mid-T metamorphic conditions. These metamorphic rocks belonged to the lower plate during the Variscan intra-Gondwana subduction but experienced much less burial than the high-P metamorphic belt.

The autochthon has been divided into the Albariza-Bembézar Succession and the Azuaga Formation. The Albariza-Bembézar succession includes quartz-muscovite-rich schists, garnet-bearing schists, staurolite-bearing schists andalusite-bearing schists, amphibolites, meta-sandstones and variably deformed meta-granitic rocks (Matas, Martín Parra, & Martínez Poyatos, 2015). Some layers of meta-sandstone are several hundred meters thick and show regional lateral continuity. The meta-granitoids range between fine and coarse-grained. Some are orthogneisses *sensu stricto*, among which are augen varieties (sample UC-1). The Azuaga Formation includes Cambrian thin-bedded phyllites and meta-sandstones.

2.4. Syn-Orogenic Rocks: Strata and Igneous Rocks

This group comprises rocks whose protoliths or the rocks themselves were formed during the Variscan Orogeny. They can be divided into two categories: (meta-)sedimentary and igneous. The sedimentary rocks were deposited in basins formed as the Variscan orogen evolved, either during contraction- or extension-dominated pulses. Some sedimentary rocks, especially the oldest ones, experienced low-grade (greenschist facies) metamorphism. The igneous ensemble comprises many Carboniferous rocks that intrude sections of the upper and lower plates and range between granitic and gabbroic terms. This ensemble also includes volcanic terms (acid to basic), some occurring within the syn-orogenic strata.

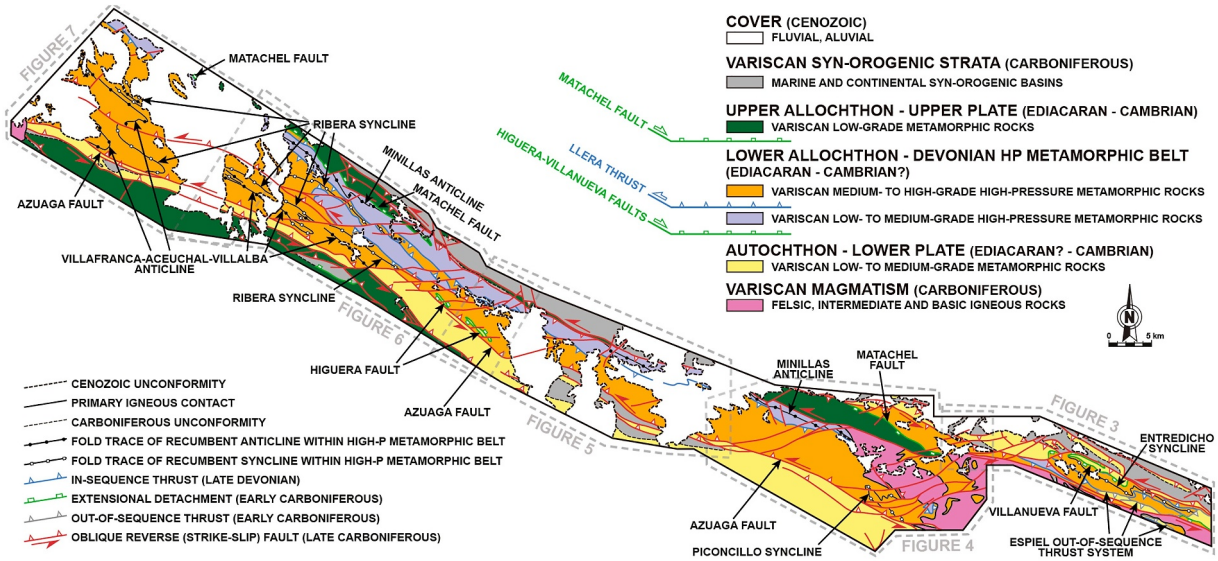

Figure 2. Regional synthesis of the main structures and tectonostratigraphy of the study area. The boundaries of the maps presented in Figures 3–7 are indicated.

3. Materials and Methods

Geological mapping was carried out on a 1:25,000 scale and assisted by a rugged tablet with GPS and GIS technologies. Base maps (topographic and orthophotos) were obtained from the Spanish National Geographical Survey (http://centrodedescargas.cnig.es). Figure 2 shows a regional synthesis of the main structures and tectonostratigraphy of the study area. Figures 3–7 show new geological maps and cross-sections of the most representative structures (see the location of the maps in Figure 1c). These geological maps include planar structural data (only a selection of representative measurements), while the maps provided as (Figure S1 in Supporting Information S1) show the orientation of linear structures and the full collection of planar data. Large-scale structural analyses are based on field observations and a selection of domains where structures were mapped carefully. Unless otherwise indicated, the main foliation within each lithological assemblage was the reference to determine and describe a lower or upper structural position across the same assemblage. The terms anticline and syncline are not based on pure stratigraphic criteria but on the rock ensemble's upper/lower structural position before folding (e.g., rocks structurally on top before folding would conform to syncline cores). Sections as normal as possible to the local vorticity vector (roughly parallel to the stretching lineation in this study) were used to determine the shear sense in field outcrops. Structural data presentation on stereographic projections (lower hemisphere and equal area; Figure 8) was performed using Stereonet v. 11.3.1 (R.W. Allmendinger, https://www.rickallmendinger.net/stereonet; Cardozo & Allmendinger, 2013). The structural data are accessible online (Díez Fernández, 2024).

Zircon grains were separated from 9 samples of meta-sedimentary and meta-igneous rocks using conventional crushing and magnetic separation techniques. Zircon fractions were handpicked under a binocular microscope at the Instituto Geológico y Minero de España (Spain). The selected zircon grains were mounted in epoxy resin and polished to expose grain centers. Cathodoluminescence (CL) images were captured (Figure S2 in Supporting Information S1), and a combination of transmitted and reflected-light optical imagery was used to select the clearest and least fractured rims of the zircon crystals as suitable targets for SHRIMP and Laser Ablation analyses. The IsoplotR program was used for data processing and production of Wetherill Concordia plots (Vermeesch, 2018), presented in Figure 9. Concordia and mean ages were calculated using highly concordant (<5% discordance) analyses.

Selected zircon grains from 3 samples (UC-1, 2 and 5) were analyzed using a SHRIMP IIe/mc instrument at the IBERSIMS ion microprobe facility (University of Granada, Spain). We followed the analytical protocol and data reduction methods described by Bea et al. (2016). The analytical results are provided as (Table S1).

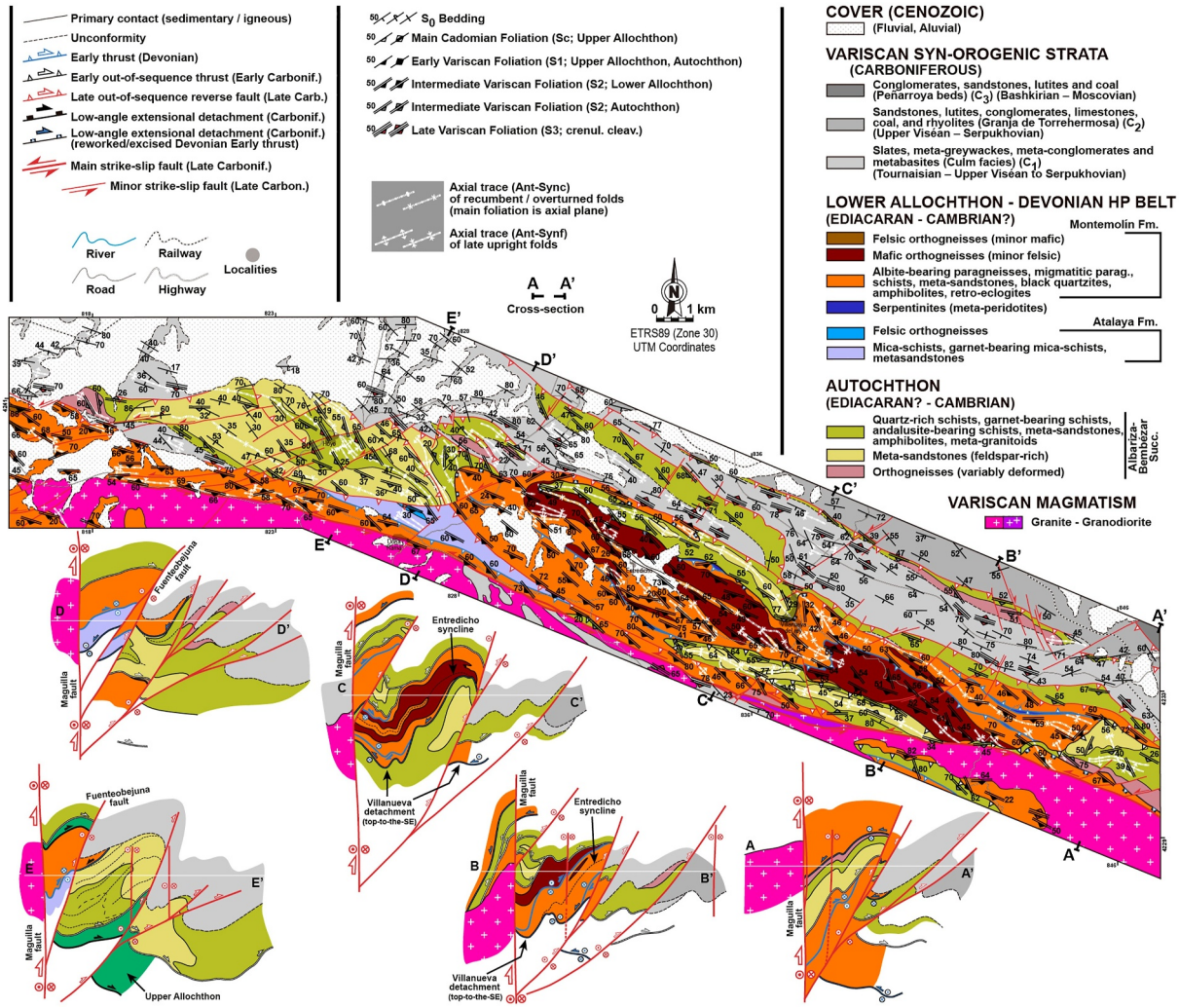

Figure 3. Geological map and cross-sections around Villanueva del Rey. The regional location is indicated in Figures 1 and 2.

Zircon grains from six samples (UC-3, 4, 8, 10, 11 and 12) were analyzed using LA-ICP-MS. The U–Pb analyses were carried out in the mass spectrometry services of ANDALCHRON SCT using a ThermoFisher iCap RQ® ICP–MS coupled to a Teledyne–Photon Machines IRIDIA® 193-nm laser platform with a high-performance COBALT® ablation chamber. We followed the analytical protocol and data reduction methods described by Ouabid et al. (2017). The specifics and analytical conditions regarding the LA-ICP-MS analyses are provided as (Text S1 in Supporting Information S1) along with the analytical results (Table S2).

4. Current Structure of the Subduction Complex: Map and Structural Analysis

Several phases of deformation affect the rocks that define the Variscan intra-Gondwana subduction complex. Some are exclusive to a single piece of the subduction system (e.g., the high-P metamorphic belt), but others affect the whole system. Due to the latter deformation's complexity and penetrativeness, the presentation of the main structures will follow a reverse chronological order.

4.1. Late Strike-Slip Systems

The youngest Variscan large-scale structures affect all the metamorphic rocks. They conform to a set of left-lateral, strike-slip faults that strike NW-SE (Figure 10a), as indicated by their mapping (Figures 1b, 1c and 2–7) and slickensides (Figure 8a). These faults range between near-vertical and high-dipping, either to the NE or SW (Figure 8a and cross-sections in Figures 3–7). The hanging wall to the high-dipping faults includes a

10.1029/2025TC008952

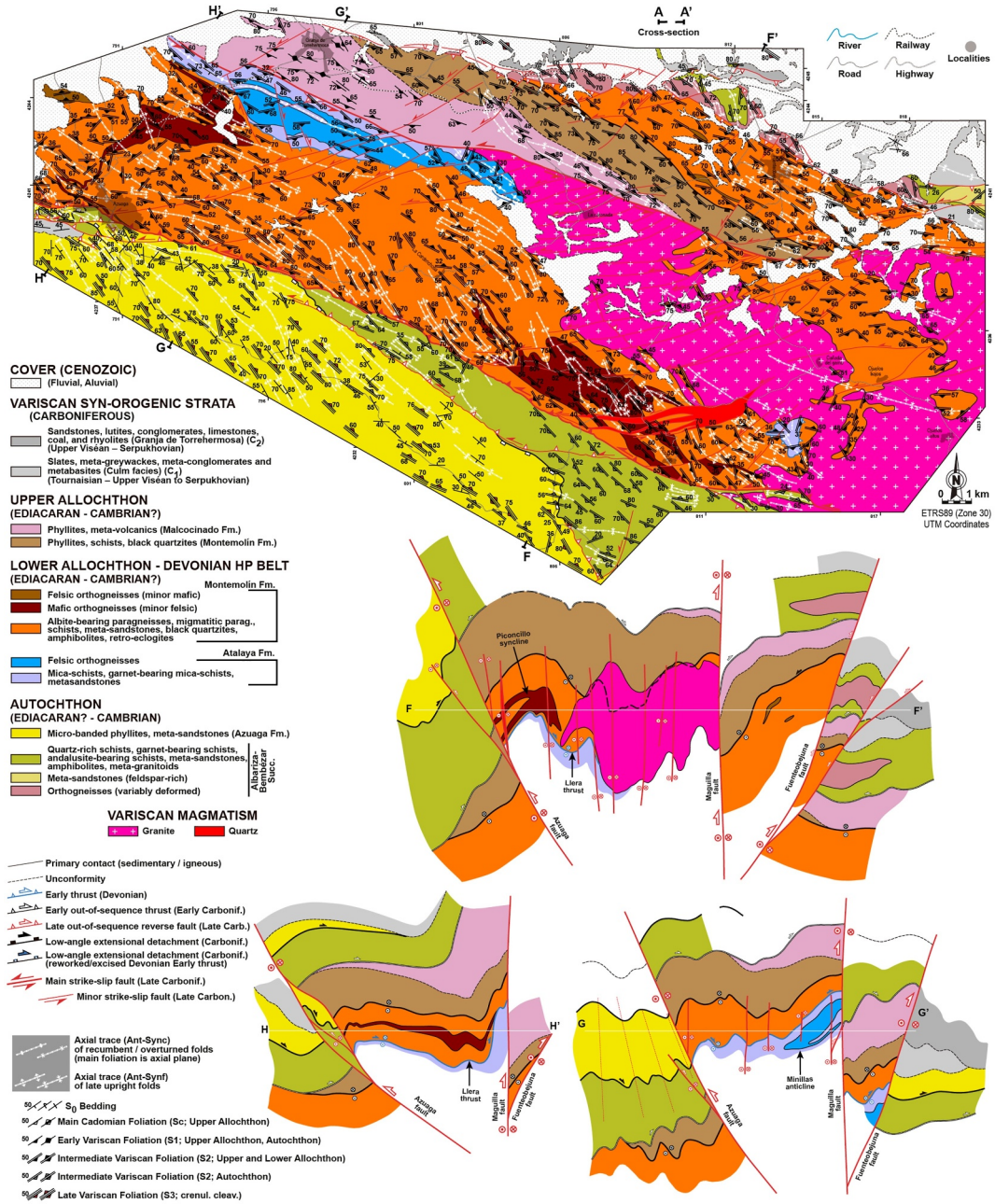

Figure 4. Geological map and cross-sections around Fuenteobejuna and Azuaga. The regional location is indicated in Figures 1 and 2.

component of upward throw, that is, they are dip-slip faults with reverse movement. Slickenlines are dominantly low SE-plunging in NE-dipping faults (Figure 8a), but we could not observe slickenlines in SW-dipping faults. The late faults are accompanied by numerous left-lateral faults striking E-W to NE-SW that define local transfer-fault (e.g., Figure 3) and tear-fault systems respect to the NW-SE faults.

The main foliation and many lithological contacts (either primary or previous faults) depict upright folds that trend similarly, if slightly oblique, to the trace of the strike-slip faults described above. The obliquity of these folds is dominantly clockwise from the trace of the faults. Such antiforms and synforms tend to occupy the hanging wall and footwall to the high-dipping reverse faults, respectively. Also, these folds may define anticlinoria, synclinoria, or even *en echelon* fold sets (see cross-sections in Figures 3–7). These folds show a near-vertical

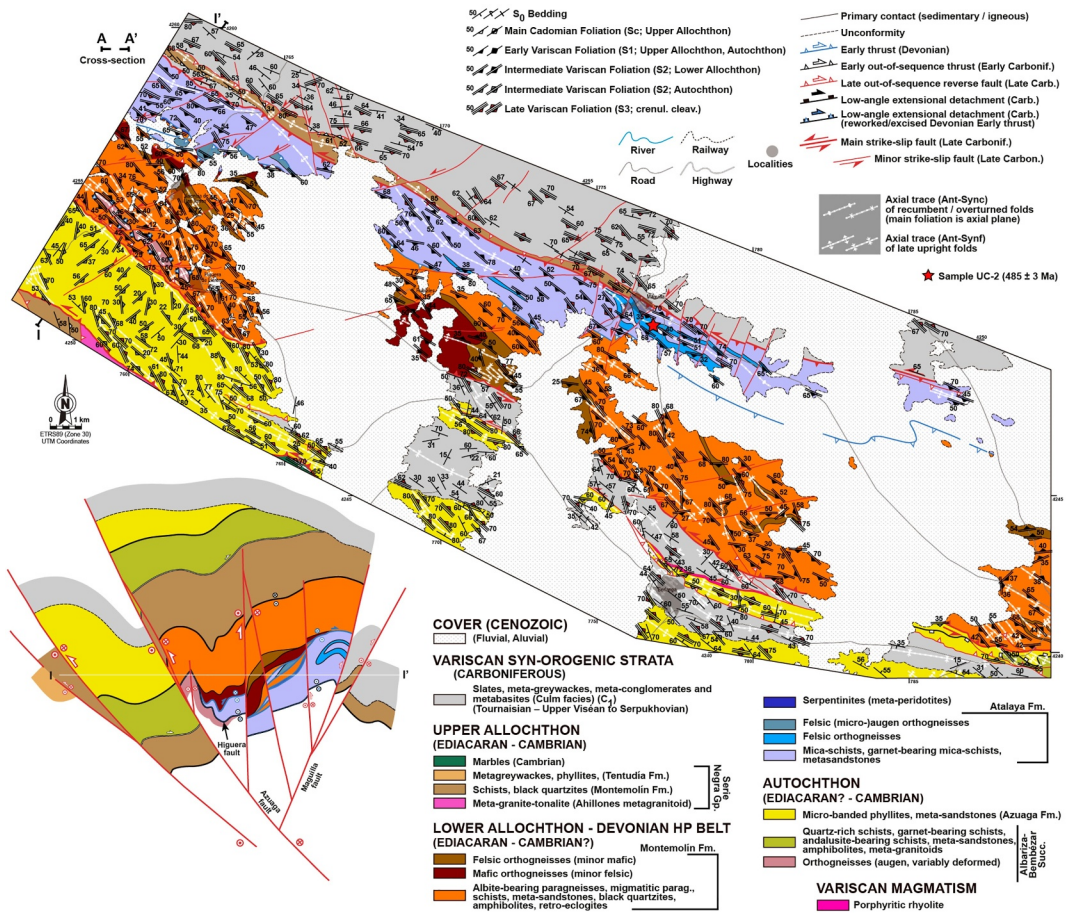

Figure 5. Geological map and cross-sections around Berlanga. The regional location is indicated in Figures 1 and 2.

crenulation cleavage (Figure 10b; see description in Section 4.7). This cleavage is accompanied by a low-plunging crenulation lineation formed at the expense of previous foliations (Figure 10b). These fold's plunge changes repeatedly across structure, being either to the SE or NW (Figure 8b). These changes can also be tracked via the geometry of fold closures defined by the main foliation, lithological contacts and bedding, collectively (Figures 8c and 8e). At the large scale, this late strike-slip system defines a positive flower structure cored by the high-P metamorphic belt and a variably disrupted anticlinorium (see cross-sections in Figures 3–7). In the vicinity of some of these faults, a local crenulation cleavage may affect any of the fabrics above (Figure 8d). This fabric represents the latest pulse of deformation recorded in the study area. It could represent the reactivation of previous structures.

This type of shear zones and folds are common in the Iberian Massif and in the rest of the Variscan Orogen (Faure et al., 2008; Martínez Catalán et al., 2020; Matte, 2001; Schulmann et al., 2014). In SW Iberia, they deform granitic rocks dated at c. 318 Ma (Pereira, Silva, et al., 2010) but are cut by granitic rocks dated at c. 306 Ma (Solá et al., 2009). Accordingly, they are considered Pennsylvanian in age (~318–306 Ma; Moscovian through to Gzhelian).

4.2. Extensional Structures

This set of structures emerges from recognizing normal faults that affect Tournaisian–Visean syn-orogenic rocks and/or are affected by the upright folds and late faults described above (Section 4.1). These extensional faults can define the contacts of the syn-orogenic rocks with the upper plate, the high-P metamorphic belt with the upper plate, and the high-P metamorphic belt with the autochthon. These extensional faults cut across the internal structure of their hanging wall and footwall, but do not distort any previous tectonic stacking.

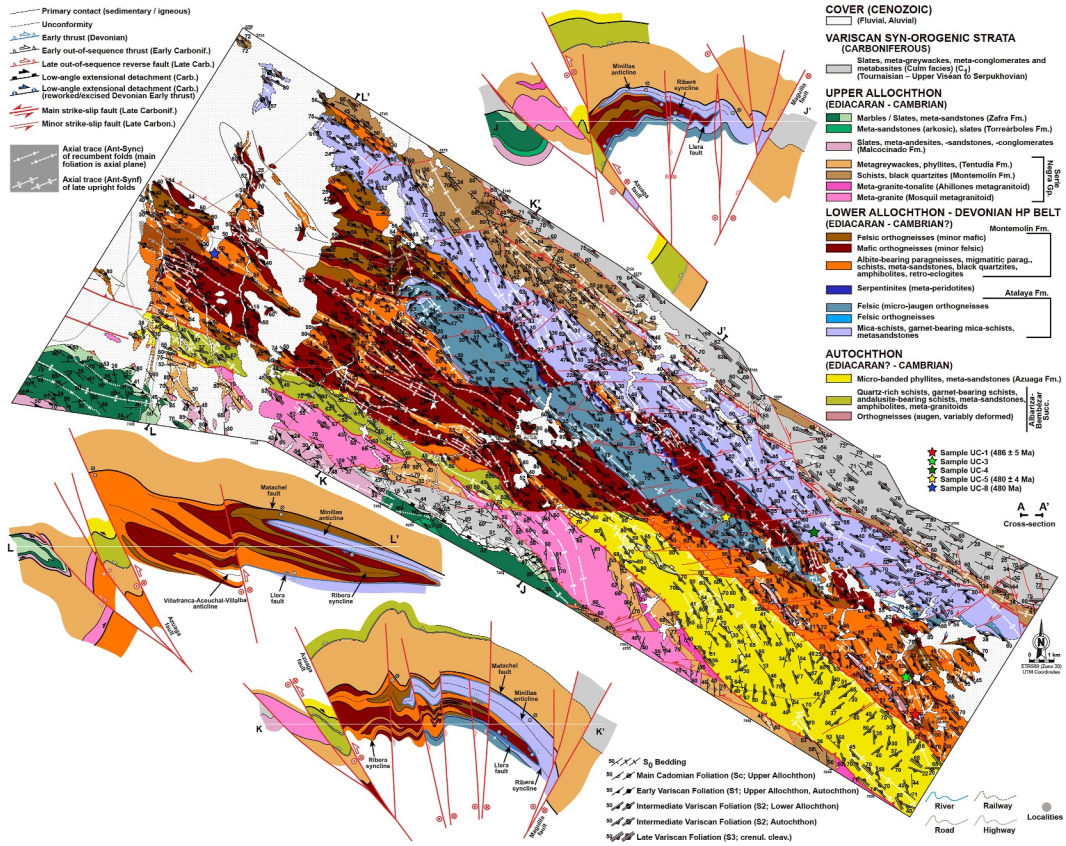

Figure 6. Geological map and cross-sections around Valencia de las Torres and Villafranca de los Barros. The regional location is indicated in Figures 1 and 2.

The Matachel fault separates the high-P metamorphic belt from the upper plate (Figure 2). The sinuous trace of this fault coincides with the axial trace of the late upright folds. Therefore, this fault was affected by them and was a moderate-to shallow-dipping fault. Kinematic criteria in phyllonites related to this fault indicate top-to-the-NW shearing (Figure 10c), with a very low-plunging stretching lineation. The cut-off points of this fault with some internal lithological contacts of the high-P metamorphic belt suggest that the Matachel fault excises progressively lower structural levels of the high-P metamorphic belt to the SE, which would emerge as a primary shallow-dipping, NW-directed reverse fault or, alternatively, as a flat-lying NW-directed fault excising the oblique, NW-dipping internal structure of an exhuming high-P belt.

The Higuera fault (Figure 2) keeps the high-P metamorphic belt on top of the autochthon, which crops out in two consecutive tectonic windows formed after late upright folding (Figures 5 and 6). The core of this extensional fault is defined by an ultramylonite that is up to ∼150 m thick and is characterized by strongly oriented quartz, muscovite, biotite, K-feldspar and plagioclase porphyroclasts, sillimanite, rare garnet and opaque minerals (Figure 10d). On the other hand, the Villanueva fault (Figure 2) separates the same pieces of the subduction system (Figure 3). Both the Higuera and Villanueva faults show top-to-the-SE kinematic criteria (sigma, C-S, C′ structures, and mica fish; Figure 10d). The trace of the Villanueva fault cuts lower structural levels of its hanging wall block to the SE than to the NW, as expected for a normal fault. Accordingly, the Villanueva and Higuera fault could represent different exposures of the same shallowly-dipping extensional system located at the base of the high-P metamorphic belt.

The lower structural sections of the high-P metamorphic belt include migmatitic paragneisses, which define, together with the overlying (regular) paragneisses and schists of the high-P metamorphic belt, a normal, telescoped metamorphic zonation that culminates with schists and phyllites of the upper plate. In some parts, the across-section distance between the migmatites and the schists/phyllites is less than 3 km so that this telescoping can be explained in a context dominated by crustal attenuation.

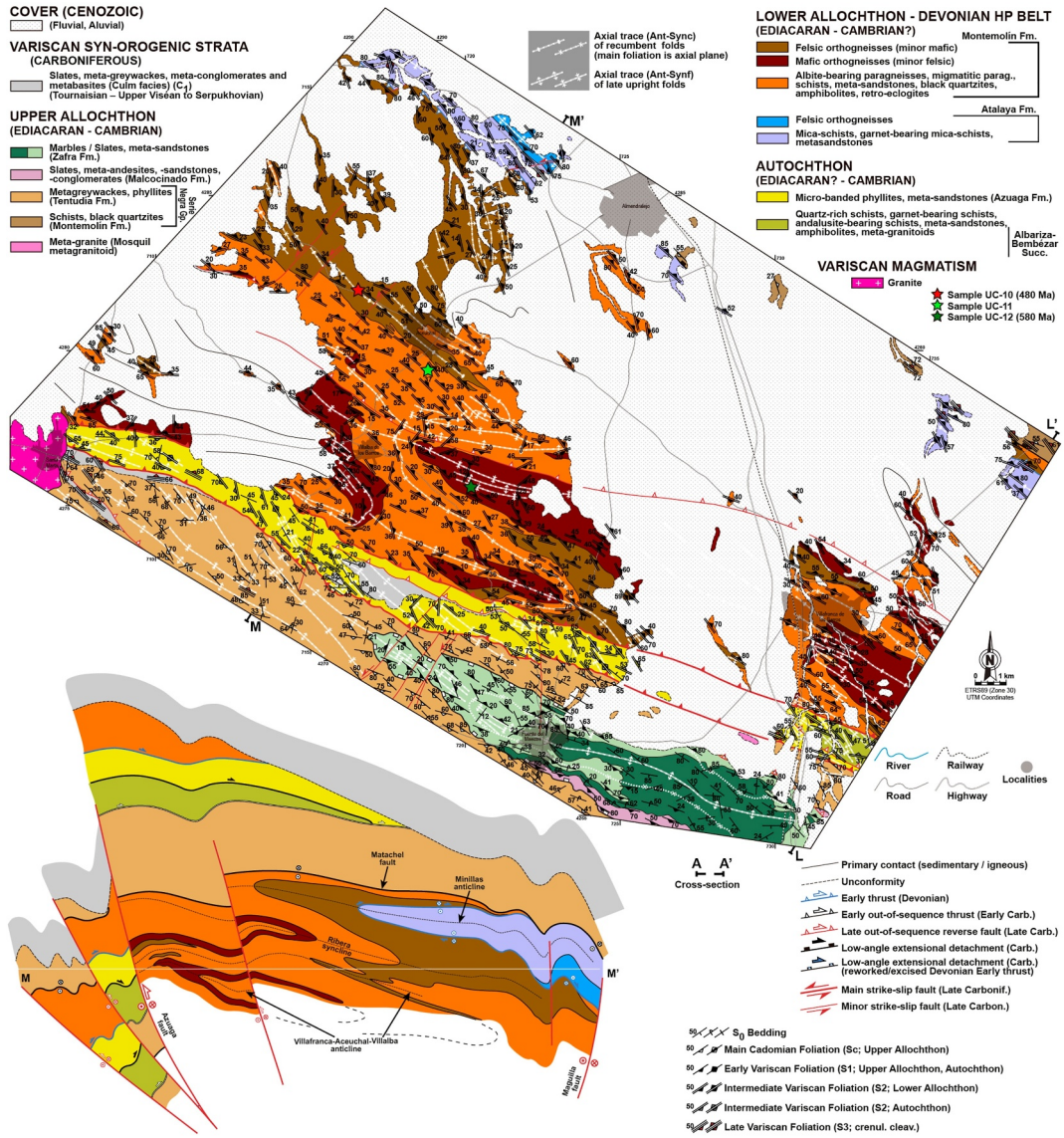

Figure 7. Geological map and cross-sections around Villafranca de los Barros and Villalba de los Barros. The regional location is indicated in Figures 1 and 2.

This extensional deformation affects the Tournaisian-Visean syn-orogenic strata, so its age should be coeval (sedimentation and extension occurred simultaneously) and/or younger. Dating the partial melting of the paragneisses in this high-P metamorphic belt (Portugal) yielded a Visean age (c. 340 Ma; Pereira, Apraiz, et al., 2010). One sample of migmatitic paragneisses analyzed in this study (UC-3) yielded similar results (see Section 5), so we consider the extension-related deformation as Visean.

4.3. Early Out-of-Sequence Thrusts

These reverse faults can be directly observed in the eastern part of the study area (Figures 2 and 3). They can be distinguished from the rest of the fault types because they are cut by the late strike-slip faults and affected by the late upright faults. Secondly, these faults juxtapose rocks of the autochthon onto the high-P metamorphic belt while keeping parts of the latter in their hanging wall. Thirdly, these faults cut across the internal structure of the high-P metamorphic belt, including internal imbricates, and lithostratigraphy. These thrusts will be considered out-of-sequence relative to the previous thrusting since they affect the high-P metamorphic belt and its contacts with the overlying and underlying units during subduction and early exhumation (see following sections).

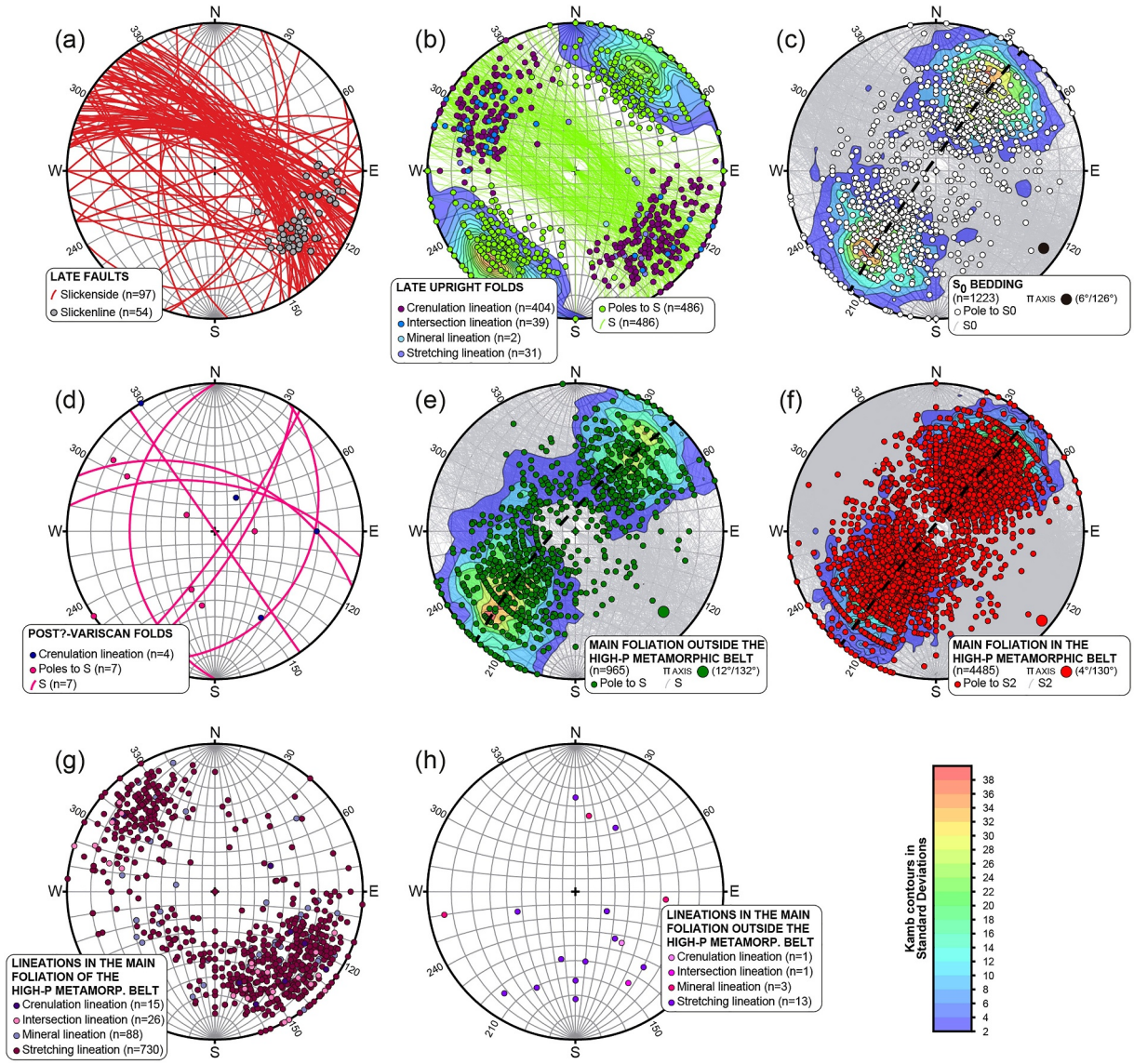

Figure 8. Stereoplots (lower hemisphere and equal area) of linear and planar structures of the study area. (a) Slickensides and slickenlines of late faults (mostly strike-slip). (b) Lineations and crenulation cleavage associated with the late upright folds (late strike-slip system). (c) Bedding. (d) Crenulation lineation and lineation associated with the latest (post-Variscan?) folds. (e) Main foliation outside the high-P metamorphic belt, including Autochthon and Upper Allochthon. (f) Main foliation in the high-P metamorphic belt (i.e., Lower Allochthon). (g) Lineations observed within the main foliation of the high-P metamorphic belt (i.e., Lower Allochthon). (h) Lineations observed within the main foliation outside the high-P metamorphic belt (mostly Upper Allochthon).

The extent of this type of fault can also be inferred by analyzing the distribution of the autochthon with respect to the high-P metamorphic belt and upper plate combined. The cross-sections in Figures 3–7 indicate that a tectonic slice of the autochthon overlies the high-P metamorphic belt. Accordingly, the high-P metamorphic belt would occupy the footwall to a much larger out-of-sequence thrust system. This thrust system cut a previous nappe stack defined by the autochthon (below), the high-P metamorphic belt (middle) and the upper plate (on top). This out-of-sequence thrust produces the same type of distortion of the Variscan suture zone as the Espiel thrust (i.e., autochthon on top of the suture zone and upper plate; Díez Fernández, Matas, et al., 2021), so we consider it its regional prolongation to the SW, as suggested in previous works (Díez Fernández, Fernández, et al., 2021).

The age of this thrust system can be constrained indirectly using the Tournaisian-Visean syn-orogenic strata as a reference. In the study area, these syn-orogenic rocks are restricted to the exposures of the hanging wall to the out-of-sequence (Espiel) thrust, either with the upper plate or the autochthon. We suggest that the footwall to this

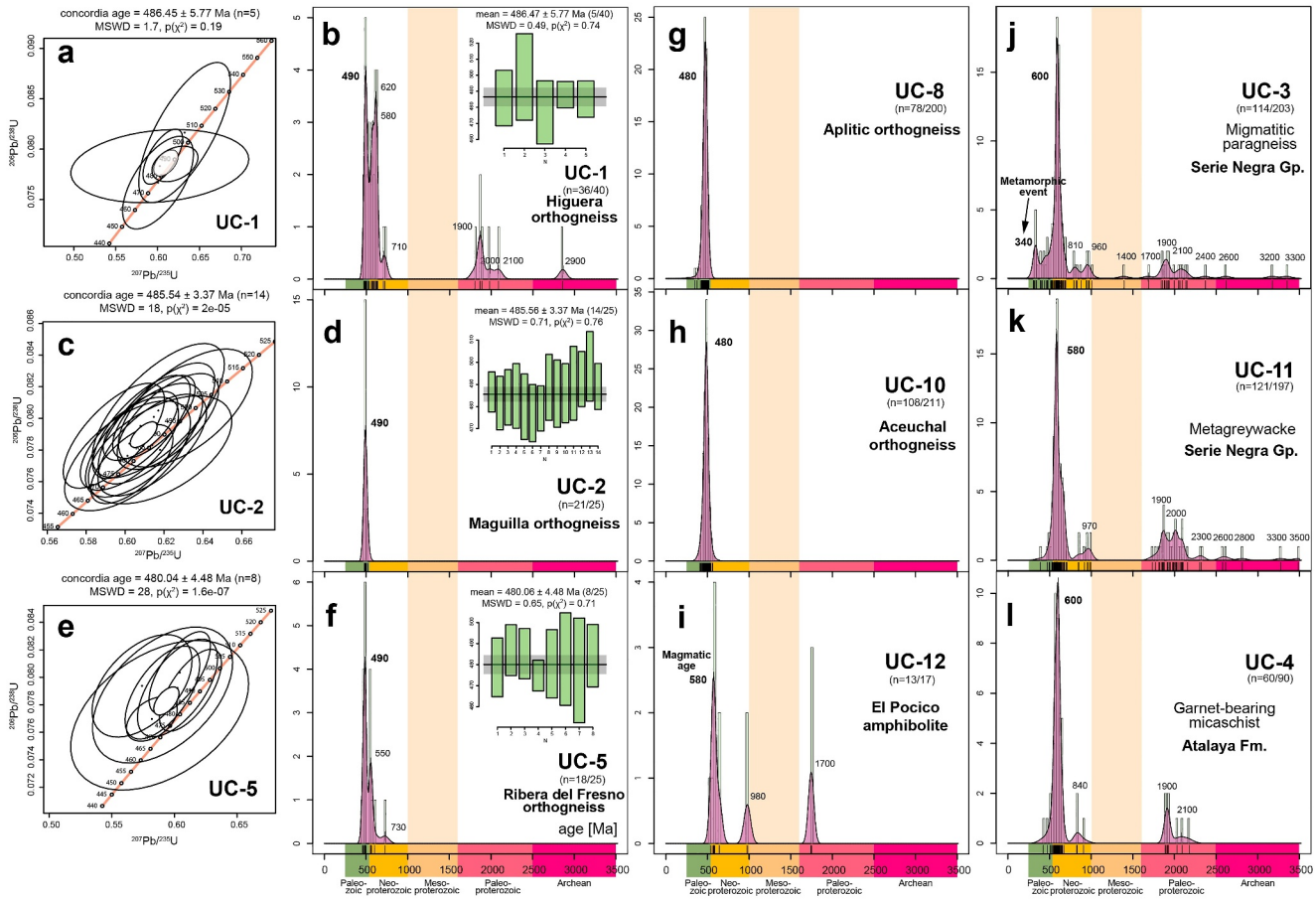

Figure 9. Geochronological results after U-Pb zircon dating of meta-sedimentary and meta-igneous rocks from the Lower Allochthon of SW Iberian Massif using (a–f) SHRIMP and (g–l) LA-ICP-MS, including Concordia diagrams (a, c, and e), weighted-mean age diagrams (b, d, and f), and probability density combined with histogram frequency diagrams (g–l).

thrust remained unexposed (by erosion) during the Tournaisian-Visean, so the age of out-of-sequence thrusting is either previous and/or coeval (Martínez Poyatos et al., 1998). The sedimentation of Serpukhovian syn-orogenic series in a contractional regime (Matas et al., 2014) is compatible with activity of this thrust system up to that age.

4.4. Recumbent Folds Within the High-P Metamorphic Belt

The internal structure of the high-P metamorphic belt is dominated by a mylonitic foliation that is axial plane to NW-SE-trending recumbent folds. This can be observed in most lithologies within the high-P metamorphic belt at the micro- (Figures 8f and 8g) and meso-scale (Figure 10e) and after a rigorous analysis of the traces of their contacts. Since most of these contacts are defined by meta-igneous rocks, and there is a lack of way-up criteria in the metasedimentary rocks due to intense strain and metamorphic recrystallization, the recognition of the major folds is based on pure geometrical analysis (e.g., Díez Fernández et al., 2017; Díez Fernández & Martínez Catalán, 2009). The cross-sections along the study area show a complete picture of the internal structure of the high-P metamorphic belt (Figures 3–7), including several synclines (Entredicho, Piconcillo, and Ribera) and anticlines (Minillas, and Villafranca-Aceuchal-Villalba) (Figure 2). These recumbent folds are bent into late upright folds, thus producing a hook-type interference pattern.

4.5. The Llera Thrust and Mantle Imbricates

The two units that define the internal tectonostratigraphy of the high-P metamorphic belt, namely the Serie Negra Gp. and Atalaya Fm., are separated by the Ribera del Fresno-Llera ultramafics (Figures 2 and 6). These metamorphosed ultramafic rocks have been interpreted by several authors as a slice of upper mantle rocks sandwiched

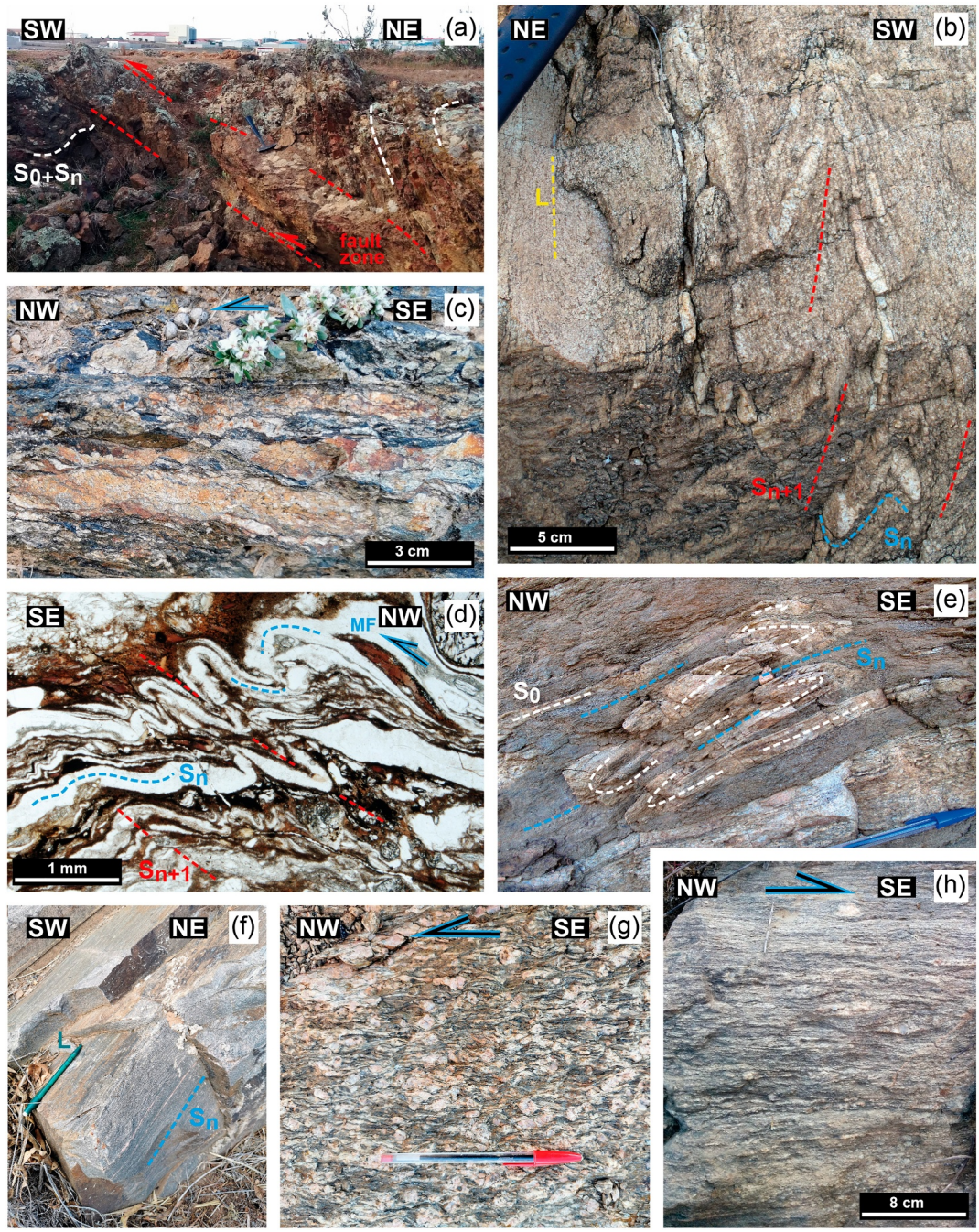

Figure 10. (a) NE-dipping fault and upright folds associated with the late strike-slip system. S_n reflects the main foliation. (b) Upright folds with accompanying crenulation cleavage (S_{n+1}) and lineation (L) that affect a previous foliation (S_n) in felsic orthogneisses of the high-P belt. (c) Mylonites with top-to-the-NW shear sense indicators (C′, sigma objects, and pressure shadows) in the Matachel fault. (d) Garnet-sillimanite-bearing augen orthogneiss (porphyroclast in the upper left corner) showing a mylonitic foliation (S_n) developed under top-to-the-SE shearing (note mica fish; MC). Sn is affected by late, asymmetric upright folds (S_{n+1} is the axial plane). (e) SE-verging recumbent folds defined by a thin layer of felsic orthogneisses (S_0) enclosed within metapelites of the high-P belt (Serie Negra Group). The main foliation (S_n) is the axial plane to the folds. (f) Mylonitic foliation (S_n) and stretching lineation (L) developed in (alkaline) orthogneisses located within the high-P belt (Serie Negra Group). (g) Augen orthogneisses (Ribera del Fresno orthogneiss, Atalaya Formation) showing top-to-the-NW kinematic criteria (sigma objects and C′-S structures). (h) Felsic orthogneisses of the high-P belt (Serie Negra Group) showing top-to-the-SE kinematic criteria (sigma objects).

in between two slices of crustal rocks, thus implying an ophiolitic nature (Ábalos et al., 2023; Chacón & Velasco, 1981). Accordingly, the boundaries of the Ribera del Fresno-Llera ultramafics correspond to major thrusts (Abalos, 1989, 1992; Apalategui et al., 1990), which will be referred to as the Llera thrust system. In the hanging wall to this thrust system is the Serie Negra Gp., which includes rocks that attained higher metamorphic grade and peak-P than those located at the footwall, namely the Atalaya Fm. (Abalos et al., 1991a, 1991b).

The geological maps presented in this work reveal that the Llera thrust system is not only restricted to the surroundings of the Ribera del Fresno orthogneiss (Figure 6) but it can also be followed farther to the north (Figure 6) and east (Figures 4 and 5), where late upright folds favor the exposure of its footwall in a tectonic window (Figure 4). Along the trace of the fault system, it can be observed several imbricates defined by alternations of serpentinites with schists and orthogneisses of the Atalaya Fm. (Figure 6) and with gneisses of the Serie Negra Gp. (Figure 6). Additional lenses of serpentinite do exist within the high-P metamorphic belt, but they tend to occur within the Serie Negra Gp. (Figure 3). These exposures are accompanied by bands that include several meters of mylonite and ultra-mylonite so that the serpentinites can be ascribed to shear zones. We could not directly connect any of these individual shear zones to the trace of the Llera thrust system. Still, the closeness between them, the sequence of superimposed structures, and the occurrence of serpentinite suggest they may be part of the same thrust system.

The kinematics of this thrust system will be discussed in the light of additional microstructural data (see Section 4.7). However, the Llera fault system cut the internal lithological contacts of its hanging wall and footwall (note cross-sections in Figure 6). The micaschists of the Atalaya Fm. (i.e., the footwall) wedges to the S around the tectonic window defined by the Ribera del Fresno orthogneiss (Figure 6). Also, the thickness of the Serie Negra Gp. (i.e., the hanging wall) enlarges towards the S and SW in that area. These two geometrical properties are typical of a frontal thrust ramp in a N-NE-directed thrust system.

This fault system is affected by both the late upright folds (Figure 6) and the recumbent folds described in the previous section (note its duplication by the Ribera syncline and the Minillas anticline; Figure 6). Accordingly, the age of this thrust system must be younger than the youngest protolith involved in the high-P metamorphic belt and cut by this thrust (e.g., Ordovician felsic gneisses of the Atalaya Fm.) and older than the recumbent folding. The age of thrusting should also be younger than the peak-P metamorphism (high-P *s.l.*) recorded in its hanging wall. It must also be synchronous to younger than the peak-P metamorphism in its footwall (i.e., Devonian; Abati et al., 2018) because this thrust inverted such record (higher-P on top; see Section 4.7). Overall, the Llera thrust must be Variscan in age, most likely Devonian-Carboniferous (see Section 7).

4.6. Recumbent Folds Outside the High-P Metamorphic Belt

The rocks that belong to the Upper Allochthon are affected by recumbent folds. Mapping and way-up criteria have allowed the recognition of a refolded, NW-SE-trending recumbent syncline (cross-section L-L′ in Figure 6). This fold likely belongs to the SW- and NE-verging train of folds that formed under low-grade metamorphic conditions in the Upper Allochthon during the Devonian, at the onset of the Variscan Orogeny in the Ossa-Morena Complex (e.g., Díez Fernández et al., 2019; Expósito et al., 2002; Expósito et al., 2003; Martínez Poyatos et al., 1995; Moreno-Martín et al., 2025).

A combination of way-up criteria, geological mapping, and obliquity between bedding and axial plane foliation has allowed the recognition of a phase of deformation including recumbent folds in the autochthon (cross-sections D-D′ and E-E′ in Figure 3). These recumbent folds belong to a NE-verging train of folds that formed under low-to mid-grade metamorphic conditions during the Devonian and can be observed in several exposures of the autochthon to the north of the study area (Díez Fernández et al., 2021b, 2024).

4.7. Microstructural Analysis

Previous works provide extensive petrographic descriptions of the main fabrics and metamorphic conditions for their development (Abalos, 1989, 1992; Abalos & Eguiluz, 1991; Abalos et al., 1991a, 1991b) (see compilation in Figure 11). Here, we will focus on critical characteristics to offer an integrated structural model based on a combined analysis of macro-, meso-, and micro-structures.

Each piece of the Variscan subduction system experienced a different evolution, which will be dealt with in the following subsections. However, they all followed a similar path regarding the late strike-slip systems. This

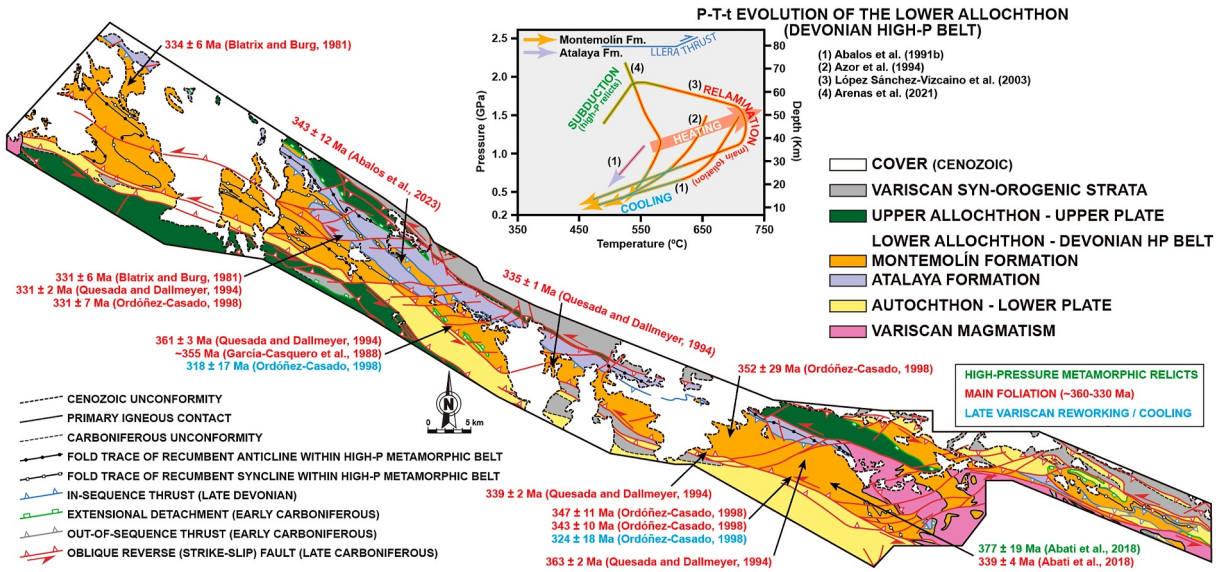

Figure 11. Geological sketch (as in Figure 2) showing the ages of Variscan metamorphism within the Lower Allochthon (Abati et al., 2018; Ábalos et al., 2023; Blatrix & Burg, 1981; García Casquero et al., 1988; Ordóñez Casado, 1998; Quesada & Dallmeyer, 1994) and a synthesis of its metamorphic evolution according to previous works (Abalos et al., 1991b; Arenas et al., 2021; Azor et al., 1994; López Sánchez-Vizcaíno et al., 2003). The lines representing the P-T paths are color-coded. Orange lines represent rocks located at the hanging wall to the Llera thrust, most of which experienced high-T metamorphism during relamination. The purple line represents rocks located at the footwall to the Llera thrust. The inner part of the lines mentioned above is also color-coded. The green section represents the subduction stage, while the red and blue sections account for the relamination stage and subsequent cooling, respectively. The ages are divided into three main groups following the tectonic evolution of the Lower Allochthon described in this work. The ages referring to the onset of high-P metamorphism are colored in green (subduction stage). The ages referring to the development of the main foliation are colored in red (early exhumation and relamination stage). The ages referring to later events are colored in blue (late strike-slip tectonics and cooling stage).

means all the rocks affected by late strike-slip shearing developed an axial plane crenulation cleavage (primary slaty cleavage in the case of syn-orogenic metasedimentary rocks), including neoblastic quartz, muscovite, chlorite, and sericite, plus reoriented minerals from previous fabrics. This fabric formed under greenschist facies conditions (2–5 kbar; Abalos et al., 1991a; López Sánchez-Vizcaíno et al., 2003), is axial plane to the upright folds described in Section 4.1 and contains a mineral lineation defined by muscovite, chlorite, and sericite. The lineation trends NW-SE and shows variation in its plunge to the SE and NW (Figure 8b). The crenulation cleavage is accompanied by a crenulation lineation that shows similar trend and variation in plunge as the mineral lineation (Figure 8b). All of the fabrics that predate this deformation are folded into upright folds, which exert strong control over the strike of previous foliations and bedding (Figures 8c–8f).

4.7.1. Upper Allochthon (Upper Plate)

The Upper Allochthon shows three foliations. The youngest foliation corresponds to the fabric related to the late Variscan strike-slip systems (see section above). In the Cambrian rocks, the previous foliation is a phyllitic to slaty cleavage developed in the chlorite zone (Figure 8e), whereas in the Ediacaran rocks this foliation is a crenulation cleavage. This fabric is axial plane to the Devonian recumbent folds described in Section 4.6 (Figure 8h).

In the Ediacaran and Cambrian rocks, the oldest foliation that can be recognized in the field ranges between phyllitic cleavage and schistosity. In the Cambrian rocks, this foliation developed in the chlorite zone, while in the Ediacaran rocks, it was developed within the biotite zone (normal metamorphic zonation). This foliation is pre-Variscan (i.e., older than the oldest Variscan deformation) and presumably formed in the context of lower Paleozoic extensional tectonics (e.g., Díez Fernández, Arenas, et al., 2022; Expósito et al., 2003; Moreno-Martín et al., 2023).

4.7.2. Lower Allochthon (High-P Metamorphic Belt)

The rocks of the high-P metamorphic belt show a penetrative and mylonitic foliation i.e., in most cases, the main single fabric observed at the outcrop scale (e.g., main foliation in Figures 10e–10h). The main foliation is parallel to the elongate shape of meta-igneous bodies and bedding, but it also can be seen as an axial plane foliation of recumbent folds both at the outcrop (Figure 10e) and map scale (Figure 6). These folds trend parallel to the current trace of the high-P metamorphic belt (i.e., NW-SE), as constrained after the macrostructural analysis in Section 4.4 and in situ measurements (Figure 8g). The main foliation post-dates Devonian (∼380 Ma), blueschists to eclogite facies metamorphism (subduction) (Abalos et al., 1991b; Abati et al., 2018; Arenas et al., 2021; López Sánchez-Vizcaíno et al., 2003) and developed under amphibolite to greenschist facies conditions (6–12 kbar; Abalos et al., 1991b; Arenas et al., 2021; López Sánchez-Vizcaíno et al., 2003; Pereira, Apraiz, et al., 2010). The main foliation accounts for the early exhumation after Devonian peak-P (>20 kbar) metamorphism, and its age is early Carboniferous (355–340 Ma; García Casquero et al., 1988; Pereira, Apraiz, et al., 2010). Previous works provided individual petrographic descriptions of the main foliation observed in each high-P metamorphic belt's lithology (e.g., Abalos, 1990; Azor, 1994; Pereira, 1999, among others). The metasedimentary rocks (micaschists) of the Atalaya Fm. seem to have experienced lesser burial and heating (9–10 kbar and 520–540°C; Abalos et al., 1991a) than the gneissic rocks of the Serie Negra Gp. (>20 kbar; Arenas et al., 2021; López Sánchez-Vizcaíno et al., 2003), which even reached partial melting conditions at high-P conditions (850–880°C at ∼16 kbar; Pereira, Apraiz, et al., 2010). Overall, the Atalaya Fm. can be considered a shallower and colder piece of the subduction system compared to the high-P rocks of the Serie Negra Gp. (Figure 11).

The minerals forming the main foliation in the Lower Allochthon metasedimentary rocks and the metabasites are aligned to define a mineral lineation. In the meta-granitic rocks (orthogneisses), the main foliation includes a stretching lineation marked by elongated grains (quartz ribbons, feldspar, plagioclase, and ferromagnesian minerals) and aggregates of mafic minerals (Figure 10f). The long axis of metabasite lenses, enclaves, and metasedimentary xenoliths included in the orthogneisses is parallel to the local stretching lineation. It so is considered a marker of the stretching lineation elsewhere. The trend of the mineral and stretching lineation does not differ from one another. Statistically, the trend of these lineations is roughly parallel to the current trace of the high-P metamorphic belt, that is, NW-SE, with the exception of some sites where the lineation trends perpendicular to the metamorphic belt (Figure 8g). However, there exist numerous cases where this lineation trends obliquely to the high-P metamorphic belt (i.e., ∼N-S), mostly clockwise from it (Figure 8g).

The main foliation includes numerous kinematic indicators such as sigma objects, C-S, and C′-S structures. The presence of such asymmetric structures is independent of the structural level. They occur mostly everywhere in the high-P metamorphic belt. However, the shear sense that can be inferred from them changes dramatically across the structure. The main foliation in the Atalaya Fm. (footwall to the Llera thrust) is consistently dominated by top-to-the-NW shear sense criteria (Abalos, 1989, and own observations; Figure 10g) (>95% of total observations). The high-P rocks of the Serie Negra Gp. (hanging wall to the Llera thrust) show an evident relative abundance in top-to-the-SE kinematic criteria (∼70% of total observations; Figure 10h), but top-to-the-NW criteria can sometimes be observed, especially in the vicinity of the Llera thrust.

4.7.3. Autochthon

The main foliation in the rocks of the autochthon shows a pattern somewhat analogous to the upper plate rocks. In the Azuaga Fm., the main foliation is a phyllitic cleavage that is axial plane to overturned folds (not recognized at a larger scale in the study area). In nearby areas, these folds also affect Devonian strata (Díez Fernández, Matas, et al., 2021), i.e., are Variscan in age. In the Devonian rocks, this foliation represents the oldest deformation associated with metamorphism. In the metapelitic rocks, this main foliation is defined by a mineral assemblage including quartz + plagioclase + muscovite ± biotite ± garnet. In the Albariza-Bembézar Succession, the main foliation ranges between a schistosity and gneissic banding, mainly parallel to bedding. In the metapelites, this foliation is variably transposed by a crenulation cleavage similar to the main foliation in the Azuaga Fm., locally producing NE-verging overturned folds (e.g., cross-sections D-D′ and E-E′ in Figure 3) developed under greenschists facies conditions (garnet-biotite zone). The main foliation, including garnet-staurolite-andalusite in the metapelites, was formed under low-P conditions and was transposed by a metamorphic event (formation of kyanite-bearing rocks) formed under mid-P conditions (Solís-Alulima et al., 2023). As in the upper plate, the rocks of the autochthon that occupied a lower structural position before Devonian folding seem to have retained

pre-Variscan metamorphic fabrics, despite all of the autochthon was buried and variably metamorphosed during the Variscan Orogeny.

5. Age and Provenance of the Protoliths of Subducted Rocks (U-Pb Zircon Dating)

The SHRIMP and LA-ICP-MS U-Pb zircon dating results are reported as supplementary data in Tables S1 and S2 files, respectively, and presented in Figure 9.

5.1. Higuera Orthogneiss (UC-1; SHRIMP)

136 zircon grains were obtained, 38 were selected, and 40 analyses were conducted. The youngest age population defined by the whole set of 36 concordant analyses peaks at 490 Ma, while the youngest set of five concordant analyses clusters around a concordia age of 486 ± 5 Ma (Figure 9a) and pool together to define a mean age of 486 ± 6 Ma (late Cambrian-early Ordovician; Figure 9b). This result is considered the best estimate for the crystallization age of the protolith.

Thirty-one analyses of xenocryst cores, non-xenocrystic inner zones, or even discordant rims yield ages spanning from 535 (Cambrian) to 2,863 Ma (Archean), which are considered inheritance. Of the 31 inherited ages, the most important populations are 620–600 Ma, 710 Ma (Neoproterozoic), and 2,100–1,900 Ma (Paleoproterozoic). Other inherited components are only represented by one analysis (Figure 9b).

5.2. Maguilla Orthogneiss (UC-2; SHRIMP)

A total of 205 zircon grains were obtained, 25 zircon grains were selected, and 25 analysis points were carried out. Twenty-one concordant analyses define a single age population peaking at 490 Ma, while the youngest set of 14 concordant analyses clusters around a concordia age of 485 ± 3 Ma (Figure 9c) and pool together to define a mean age of 485 ± 3 Ma (early Ordovician; Figure 9d). This result is considered the best estimate for the crystallization age of the protolith.

5.3. Ribera del Fresno Orthogneiss (UC-5; SHRIMP)

A total of 183 zircon grains have been obtained, of which 24 have been selected, and 25 analysis points have been carried out. The youngest age population defined by the whole set of 18 concordant analyses peaks at 490 Ma, while the youngest set of eight concordant analyses clusters around a concordia age of 480 ± 4 Ma (Figure 9e) and pool together to define a mean age of 480 ± 4 Ma (early Ordovician; Figure 9f). This result is considered the best estimate for the crystallization age of the protolith.

Ten analyses of xenocryst cores, non-xenocrystic inner zones, or even discordant rims yield ages from ~730 to ~550 Ma (Neoproterozoic), considered inheritance. Of the 10 inherited ages, the most important population is 550 Ma. Other inherited components are only represented by one analysis (e.g., 730 Ma; Figure 9f).

5.4. Aplitic Orthogneiss (UC-8; LA-ICP-MS)

A total of 200 zircon grains have been obtained and analyzed. The youngest and single-age population defined by the whole set of 78 concordant analyses peaks at 480 Ma (early Ordovician), which is considered the best estimate for the protolith's crystallization age (Figure 9g).

5.5. Aceuchal Orthogneiss (UC-10; LA-ICP-MS)

A total of 211 zircon grains have been obtained and analyzed. The youngest and single-age population defined by the whole set of 108 concordant analyses peaks at 480 Ma (early Ordovician), considered the best estimate for the protolith's crystallization age (Figure 9h).

5.6. El Pocico Amphibolite (UC-12; LA-ICP-MS)

A total of 17 zircon grains have been obtained and analyzed. This sample provided three age peaks after 13 concordant analyses. The youngest age peak is defined by eight analyses that cluster around 580 Ma (Ediacaran), which is considered the crystallization age of its protolith (Figure 9i). The other age groups correspond to early Neoproterozoic (980 Ma) and Paleoproterozoic (1,700 Ma) clusters.

5.7. Serie Negra Gp. Migmatitic Paragneiss (UC-3 and U-11; LA-ICP-MS)

A total of 203 zircon grains have been obtained and analyzed from migmatitic paragneisses (UC-3). 114 analyses yielded concordant ages, which are distributed in several age populations. The youngest age peak is 340 Ma (Visean; Figure 9j), which matches the Variscan metamorphic peak (partial melting) of similar paragneisses in other sections of the high-P metamorphic belt (Pereira, Apraiz, et al., 2010). The second youngest peak is 600 Ma (Ediacaran), defined by abundant analyses (Figure 9j). This is considered the maximum depositional age of the sedimentary protolith. Other age groups correspond to late Neoproterozoic (1,000–800 Ma), Paleoproterozoic (2,100–1,900 Ma), and some minor Archaean clusters (Figure 9j).

A total of 197 zircon grains have been obtained and analyzed in the metagreywackes (UC-11). One twenty-one analyses yielded concordant ages, which are distributed in several age populations. The youngest peak is 580 Ma (Ediacaran), defined by abundant analyses (Figure 9k). This is considered the maximum depositional age of the sedimentary protolith. Other age groups correspond to late Neoproterozoic (1,000–800 Ma), Paleoproterozoic (2,100–1,900 Ma), and some minor Archaean clusters (3,300–3,500 Ma; Figure 9k).

5.8. Garnet-Bearing Michaschist From Atalaya Fm. (UC-4; LA-ICP-MS)

A total of 90 zircon grains have been obtained and analyzed. Sixty analyses yielded concordant ages, which are distributed in three age populations. Most of the analyses define the youngest age peak, which clusters around 600 Ma (Ediacaran; Figure 9l). This could represent the maximum depositional age of the sedimentary protolith. The other age groups correspond to late Neoproterozoic (900–800 Ma) and Paleoproterozoic (2,100–1,900 Ma) clusters (Figure 9l).

6. Assessments Regarding U-Pb Zircon Age Data

The age of the sedimentary protoliths of the Serie Negra Gp. ranges between 600 and 580 Ma (Ediacaran), that is, between the maximum depositional age constrained by zircon grains and the oldest igneous rock within it (UC-12; El Pocico amphibolites). This age and the abundance of mafic rocks make this counterpart of the Serie Negra Gp. a correlative to the Montemolín Fm. (e.g., Rojo-Pérez et al., 2022; Rojo-Pérez et al., 2024; Sánchez-Lorda et al., 2016).

The age populations defined by zircon grains of the Serie Negra Gp. (UC-3 and 11) and Atalaya Fm. (UC-4) are rather similar, except for some minor Archean clusters in the latter. The ages of the protoliths of (alkaline) meta-granitic rocks within the Serie Negra Gp. (UC-1 and 8) and Atalaya Fm. (UC-2 and 5) are roughly identical, that is, span a range between 475 and 490 Ma (late Cambrian-early Ordovician), within error. Although the series' primary petrological nature may differ (more greywackic for the case of the Serie Negra Gp.), the main sources of detritus for the Serie Negra Gp. and Atalaya Fm. seem the same. We observe this as an indication of close paleo-location, which is further supported by the subsequent (alkaline) magmatism that intruded both of them virtually at the same time. Independently from their age, these two metasedimentary series were probably deposited close to one another and remained so at least until the Ordovician. The zircon age populations are typical of the North African margin of Gondwana, around the West African Craton (Linnemann et al., 2007, 2014; Nance et al., 2008; Nance & Murphy, 1994; Stephan et al., 2019). These populations mimic the input of other meta-sedimentary series involved in the Devonian high-P metamorphic belt exposed in NW Iberia, even regarding the exiguous Stenian-Tonian input (Díez Fernández et al., 2010, 2013).

The Llera thrust cut several Ordovician orthogneisses along its trace, so its age must be younger than 480 Ma. U-Pb dating of metamorphic zircon in retro-eclogites from the high-P metamorphic belt yielded Devonian ages (Abati et al., 2018). By carrying it on top of lower-pressure rocks, the Llera thrust represents the first large-scale structure that affects the high-P record of the metamorphic belt, so the functioning of this fault must be framed into the Variscan Orogeny. After the lower Paleozoic, the African margin of Gondwana did not experience collisional deformation and metamorphism, especially under high-P conditions (e.g., Díez Montes et al., 2010; Moreno-Martín et al., 2023, 2025; Simancas et al., 2004), until the Variscan Orogeny, which validates this interpretation.

7. Restoration of Post-Subduction Deformation and Discussion of Early Exhumation Mechanisms

The only large-scale structures related to the internal dynamics of the subduction zone are the Llera thrust and the train of SE-verging recumbent folds. The thrust moved older, hotter, and deeper sections of a Variscan lower plate over younger, colder, and shallower ones (Montemolín Fm. of the Serie Negra Gp. onto Atalaya Fm.). The Llera thrust is bent into a train of recumbent folds that do not affect the underlying units. Therefore, the Llera thrust is older than the basal thrust that placed the high-P metamorphic belt onto its autochthon (i.e., the precursor of the Villanueva fault). Accordingly, major thrust propagation after subduction progressed down-structure during the early stages.

The previous assessment on the kinematics of the Llera thrust is based on pure geometrical analysis (i.e., top-to-the-N; Section 4.5). This is aligned with the microstructural kinematic criteria observed in its footwall (Atalaya Fm.) and lower parts of its hanging wall (top-to-the-NW). However, the kinematics observed in most of the hanging wall are just the opposite (i.e., top-to-the-SE). The resulting picture is analogous to the model proposed by Chemenda et al. (1995) for the exhumation of large pieces of continental crust after subduction. For the most part, this piece of continental crust would have remained internally coherent as it progressed back up, over-thrusting the lower plate (such is the case of the Llera thrust hanging wall), that is, it was not transformed into a block-in-matrix ensemble (tectonic mélange). The return of this piece of continental crust (top-to-the-N) through the slab-mantle interface would have forced an opposite, normal sense of motion (top-to-the-SE) and exhumation in its upper part (Figures 12a and 12b). The band of serpentinites (after peridotites; Ribera del Fresno-Llera ultramafics) that occur through the contact between the hanging wall and footwall developed antigorite foliation (overprinting lizardite mesh and ghost idiomorphic amphibole microstructures), which has been related to reworking under prograde high-P metamorphism (Ábalos et al., 2023). This suggests the meta-peridotites belonged to the downgoing lower plate and represent a slice of its upper mantle. If that was the case, the Llera thrust would represent a rupture of the whole crust after subduction (Figure 12b).

Eclogite is a minor constituent of the high-P metamorphic belt as it only occurs as meter-scale pods within felsic gneisses and metasedimentary rocks, which make most of the belt. Consequently, most of the rocks of the high-P metamorphic belt did not experience eclogitization (and a significant increase in density). Therefore, the sections that were exhumed represented buoyant pieces of crust buried into a much denser mantle. This density contrast probably promoted the internal rupture of the subducting crust and early exhumation. Phyllosilicate-rich rocks are mechanically weaker than rocks richer in quartz and feldspar (e.g., gneisses) and can decrease strength, anisotropy, and increase ductility with increasing mica content (Borg & Handin, 1966; Carter et al., 1964; Gottschalk et al., 1990; Shea & Kronenberg, 1992, 1993). The different composition of the series at each block of the Llera thrust implies a low-yield strength layer located at the (footwall) Atalaya Fm., which is much richer in micaschists than the hanging wall (mostly gneisses). Such pre-existing weakness, combined with buoyancy forces, could have favored the internal rupture of the crust along their primary interface. This would explain why the Llera thrust seems not to have duplicated any previous tectonostratigraphy in the region (Figure 12b).

The early exhumation of the high-P metamorphic belt, as reflected by its main foliation, proceeded up to upper mantle and lower crust depths (6–12 kbar; Abalos et al., 1991b; Arenas et al., 2021; López Sánchez-Vizcaíno et al., 2003; Pereira, Apraiz, et al., 2010; Figure 11). This path must include the Llera thrust and the generation of isoclinal recumbent folds that eventually bent this thrust. Accordingly, the top-to-the-NW and -SE shear senses observed in the main foliation should be explained in the context of the Llera thrust and in relation to fold development since this foliation represents their axial plane. Recumbent folding would have taken place later during the upward progression of the piece of subducted crust. Currently, the high-P metamorphic belt is exposed along the core of a late upright antiform defined by the main foliation of the belt (Figures 3–7) and is surrounded by pieces of the upper plate (Upper Allochthon) that extend for tens of km to the NE and SW (Figures 1c and 2). Accordingly, the high-P metamorphic belt was entirely covered by the upper plate (Upper Allochthon) during the development of the main foliation. This, plus the development of the train of isoclinal recumbent folds (significant flattening required), the metamorphic conditions of the main foliation, and the juxtaposition of the high-P metamorphic belt against the upper plate suggest that the ascending high-P block reached the base of the upper plate at some point. The SE-verging geometry of the recumbent folds at the large scale and the two opposite shear senses of the main foliation can be reconciled if the upper tip of the ascending crust docked at the upper plate. The rest of it would have continued to be sheared and progressively constrained between the upper plate and

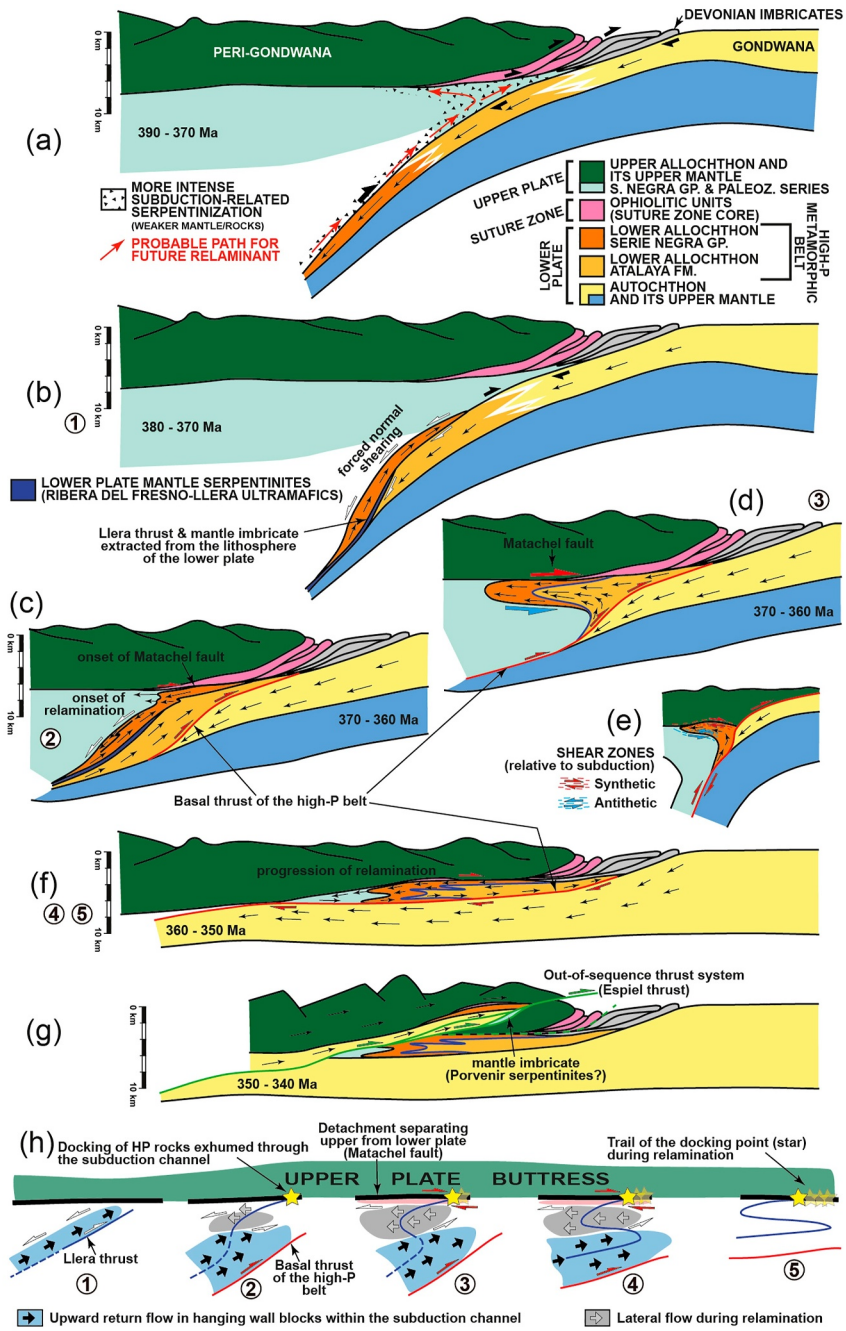

Figure 12. Tectonic model for the exhumation of the Devonian high-P metamorphic belt exposed in SW Iberia during the Devonian and Carboniferous. Thin black arrows indicate the movement of crustal rocks. Encircled numbers alongside each subsection refer to subsection (h) numbers. (a) Devonian continental subduction after the closure of an oceanic basin that separated Gondwana from a peripheral terrane. Zones affected by more intense subduction-related serpentinization are indicated. The red arrows indicate the exhumation path for the future relaminant. (b) Internal rupture within the continental slab and exhumation of a large coherent lithosphere block back through the subduction zone (onset of the Llera thrust). Note forced normal shearing at the top of the exhuming block. (c) Docking of the hanging wall block of the Llera thrust at the upper plate and onset of (relamination) subhorizontal tectonic flow of the high-P metamorphic belt beneath the upper plate. The onset of subduction-underthrusting of the Autochthon assists in the exhumation of the still-deep-seated high-P metamorphic belt. (d) The progression of the subhorizontal tectonic flow under the upper plate favored the juxtaposition of the high-P metamorphic belt against a piece of continental crust lacking of coeval high-P metamorphism. (e) Sketch illustrating the relamination of subducted continental crust (adapted from Hacker et al., 2011). Note the location of major shear zones and kinematics required for relamination to occur (further explanations in the main text). (f) Amplification of recumbent folds in the high-P metamorphic belt due to increasing narrowing exerted by the arrival of more buoyant crust upon further underthrusting of the lower plate (flatter subduction). (g) Out-of-sequence thrusting and juxtaposition of the Autochthon and other mantle imbricates (Porvenir serpentinites; Díez Fernández, Matas, et al., 2021) over the high-P metamorphic belt and upper plate. (h) A sequence of sketches that illustrates a kinematic model that fits the tectonic evolution presented above and explains the development of lithospheric-scale thrusts and large recumbent folds with opposed regional vergence.

the underlying lower plate (Figure 12c). Interestingly, the Matachel fault represents a primary top-to-the-NW shear zone, which in this context would have allowed for a displacement of the high-P metamorphic belt underneath the base of the upper plate and away from the subduction zone (Figures 12c and 12d). Collectively, the main structures formed during the early stages of high-P rock exhumation and their kinematics point to a process of tectonic underplating of continental crust (e.g., Chemenda et al., 2000). In a way, it also reminds of the caterpillar-walk proposed by Tirel et al. (2013).

Magni et al. (2017) refer to "continental underplating" after slab break-off to explain the emplacement of a vast piece of lower plate under an upper plate. In that model, it is the whole remaining and previously subducted continental crust that is underplated under the upper plate. Notably, this process occurs while the remaining subducted crust does not lose its internal coherence, and, most importantly, while the lower plate is affected by general shearing compatible with the kinematics of ongoing subduction/collision. This is at odds with our study case. Firstly, the subducted crust has lost its internal coherence to the development of the Llera thrust (which we defend it is a crustal-scale structure). And secondly, the exhumation of the high-P rocks in our study case combines synthetic and antithetic shearing, not just one shearing compatible with ongoing subduction.

The processes we propose align with the concept of relamination, particularly in the case of subducted continental crust (Hacker et al., 2011). The early exhumation of a subducted continental crust can be linked to a crustal-scale thrust with similar kinematics to ongoing subduction (Figure 12e), i.e., the Llera thrust. The displacement of the relaminant beneath the upper plate and away from the trench requires an upper shear zone with similar kinematics to ongoing subduction (i.e., the top-to-the NW Matachel fault) and a lower shear zone with opposed kinematics, that is, the dominant top-to-the-SE kinematics of the main foliation in the high-P metamorphic belt (Figure 12e). If subduction progresses, the early crustal-scale thrusts may be eventually deformed (folded, excised, etc.) between the upper-lower plate interphase, just like the relaminant. Note that the Llera thrust is affected by the same recumbent folds observed within the whole high-P metamorphic belt. The relaminated high-P metamorphic rocks should be juxtaposed against a piece of overlying continental crust lacking of high-P metamorphism (the upper plate). Interestingly, ophiolites are not expected to be found along this contact because, despite it represents a boundary between rocks derived from an upper and a lower plate, it does not account for an accretionary fault or a variably reworked version of it (i.e., the suture zone is somewhere else).

According to Maierová et al. (2018), relamination is a "process where crustal material from the lower plate is emplaced—relaminated—at the base of the upper plate and eventually form a part of the upper plate." According to Gerya (2022), "during continental collision, incoming continental crust of the lower plate can be sometimes deeply subducted, emplaced at the base of the upper plate, and eventually incorporated into its crust." This mechanism of continental-crust transformation is called relamination, and the relaminant is formed generally by buoyant felsic metasedimentary or metaigneous rocks." In our study, we are documenting the addition of previously subducted and buoyant crustal material to the base of an upper plate crust. This could also be referred to as crustal underplating (Furlong & Fountain, 1986). A relamination can occur at the bottom of the upper-plate lithosphere (sublithospheric relamination), and also at nearly the base of the upper plate crust and eventually intrude into the crust (intra-crustal relamination) (Maierová et al., 2018). However, we think this is a restricted view for the process. If the upper plate is thick and strong, the exhumation of high-P rocks would typically proceed along the plate interface after returning through the subduction channel (Guillot et al., 2009; Maierová et al., 2018; Warren, 2013). If not, the accumulation of deeply subducted material to the base of the upper plate crust under the fore-arc region (e.g., Schulmann et al., 2014) could lead to subhorizontal flow upon appropriate conditions. In our case, the upper plate would have covered the high-P metamorphic belt entirely once its high-P rocks were exhumed up to a lower crust depth (i.e., after relamination). We think this implies that the exhumation of high-P rocks did not proceed along the plate interface once these rocks reached the base of the upper plate crust. This would have been also favored by the arrival of progressively more buoyant (thicker) crust to the subduction zone (e.g., the Autochthon). Once there, the upper section of the high-P metamorphic belt flowed away from the subduction trench (i.e., to the SE) while the underlying sections still flowed synthetically to the ongoing subduction (i.e., to the NW).

Advances in understanding the dynamics of relamination have primarily relied on numerical models (e.g., Gerya et al., 2002; Gerya et al., 2008; Maierová et al., 2018; Sizova et al., 2012). These models emphasize the critical role of rheology, particularly various weakening mechanisms (deformation-, melt-, and fluid-induced), in governing tectonic evolution. Relamination requires a weakened zone, either in the mantle lithosphere (for

sublithospheric relamination) or an extremely weak upper plate (for intracrustal relamination). In both cases, the relaminant itself is significantly weakened, often due to partial melting. The subduction of oceanic and continental crust favors the release of fluids and consequent serpentinization of the mantle wedge (e.g., Hyndman & Peacock, 2003; Martin et al., 2020). The resulting serpentinites have low strength and may therefore provide a path through "weakened rocks" for a relaminant. Serpentinization is thought to be more intense along the subduction zone (favoring the occurrence of subduction channels; Guillot et al., 2009) and in the fore-arc region (e.g., Bostock et al., 2002; Hyndman & Peacock, 2003). The connection between these two sections of the mantle wedge would provide a path for buoyant material to advance upwards through the subduction channel and then beneath the upper plate crust and away from the trench (Figure 12a). According to the PTt evolution of the high-P metamorphic belt (Figure 11), the heating and partial migmatization during exhumation should have contributed to significantly weaken the relaminant. The several PTt paths calculated for the high-P metamorphic belt (Figure 11) indicate heating during the early stages of exhumation up to lower crust depths, as expected for a tectonic slice advancing towards the hot corner of the overlying mantle wedge (e.g., Sang et al., 2023; Zhou et al., 2022). The subsequent exhumation is accompanied by cooling, which would represent the stage during which the relaminant is attached under a (colder) upper plate. The Llera thrust would account for the return of deeply buried continental crust through the subduction channel up to the base of the upper plate crust. The combination of recumbent folds and paired antithetic shearing could represent the accumulation of the partially exhumed high-P rocks at the base of the upper plate crust in the fore-arc region and their displacement beneath the upper plate and away from the subduction channel. This evolution is analogous to that proposed by Schulmann et al. (2014) for the Bohemian Massif. As to the upper plate, the re-folded structure formed during the Devonian and Carboniferous indicates widespread syn-metamorphic ductile deformation. Notably, the syn-orogenic sedimentary series that covered the upper plate (deposited over the uppermost crust) were affected by deformation under greenschist facies conditions. This deformation and metamorphism are compatible with a warm upper plate, which we think it behaved as a weak block during Variscan orogenesis, like in other sections of the Variscan Orogen (e.g., Faure et al., 2025).

Although the Villanueva fault is an extensional detachment, the juxtaposition of the high-P metamorphic belt over its relative autochthon (colder, shallower, and younger) must have been carried out by a former, now dissected (reactivated?) thrust. The Variscan burial of the relative autochthon followed an intermediate P/T (Barrovian) gradient (Solís-Alulima et al., 2023). This accords well with a model in which the juxtaposition (underthrusting) of the relative autochthon occurred once the high-P metamorphic rocks had become a relaminant under the upper plate. A model in which the relative autochthon we observe today underthrusts the high-P metamorphic belt while the latter ascended through the subduction zone would require a lower P/T gradient and, most probably, evidence of higher peak-P. We cannot rule out the possibility that most of such a record in the autochthon is lost to superimposed retrogression and/or tectonic dismemberment (note the current contacts are extensional detachments). However, we should also keep in mind that the two possibilities, an earlier and higher P/T gradient and a subsequent lower P/T gradient for the autochthon, can be explained in a context in which progressively thicker (and more buoyant) lithosphere reaches the trench. Overall, this drop in the P/T gradient is reflected in the contrasted metamorphic record between the high-P metamorphic belt and its autochthon and is considered an indication of the transition from subduction to a collisional stage (e.g., Rubio Pascual et al., 2024).

The following structural record that affects the high-P metamorphic belt can be framed in a collisional stage (out of the scope of this article). The early out-of-sequence thrusting would represent a stage where the continental subduction zone no longer functions. The accretion (including relamination) and underthrusting of different terranes and sections of the Gondwana continent that governed the earlier stages may have ceased and be replaced by a thrust system that cut across the previous nappe stacking, likely via (over?)thrusting. At this point, a piece of the relative autochthon beneath the high-P metamorphic belt was brought onto the latter, and the hanging wall block of this out-of-sequence thrust system was extensively exposed to erosion (Figure 12g). We can only speculate about which could have been the reason(s) for this significant change in the orogenic dynamics. One such reason could be the processes and mechanisms by which the subducted crust was primarily exhumed. An internal rupture of the whole lithosphere (note upper mantle imbricate in the Llera thrust) implies that the remaining lower plate in the footwall to the Llera thrust would have lost an essential part of the slab pull forces that may have promoted subduction in the first place (Figure 12a). The relationships between converging plates were indeed redefined upon a scenario where the lower plate increases its net buoyancy dramatically after losing its dense root. The first of these changes is reflected in the underthrusting of moderate-P rocks (relative

autochthon) under the high-P metamorphic belt, that is, subduction was much flatter but still following an in-sequence (accretion-like) scheme (Figure 12f). The out-of-sequence thrust system implies a redefinition of the main fault planes by which the orogen is built, as they cut and duplicate the structure of the previous major faults. The way the high-P metamorphic belt and its relative autochthon are duplicated implies that major fault propagation changed from being directed towards the sections of the lower plate located away from the trench (piggyback, as expected in a subduction/accretion model) to jumping backward (overstep) to a section located at the back of the trench (i.e., in the upper plate). This could be a consequence of the reactivation and upward propagation of previous thrust ramps in the relative autochthon that, after a progressive flattening of the lower plate, became favorable planes to accommodate further shortening (Figure 12g).

Early crustal thickening gave way to pervasive extension, like in many other parts of the Variscan orogen (e.g., Dias da Silva et al., 2024; Martínez Catalán et al., 2014; Pereira et al., 2009; Rubio Pascual et al., 2013). In this particular part, it was created the extensional detachments that conform some of the mechanical contacts between pre-orogenic (e.g., Villanueva fault) and syn-orogenic rocks, together with the sedimentary basins that accumulated such rocks (e.g., Armendariz et al., 2008). Contractional deformation resumed later and led to the development of strike-slip shear zones and accompanying upright folds that reworked the whole structural set. As in the case of extension, this contractional deformation is not exclusive to the study area and is essentially ubiquitous in the hinterland of the Variscan Orogen (e.g., Abalos et al., 1991c; Díez Fernández, Fernández, et al., 2021; Díez Fernández & Pereira, 2017; Martínez Catalán, 2011; Pérez-Cáceres et al., 2016).

8. Conclusions

The initial exhumation of high-P metamorphic rocks in a Variscan continental subduction zone of SW Iberia was assisted by an intra-subduction zone lithosphere-scale thrust, referred to as the Llera thrust. The Llera thrust brought deeper sections of the continental slab onto shallower ones, including a slice of upper mantle from the lower plate. The Llera thrust proceeded up to the base of the upper plate, which behaved as a buttress and locked the exhumation path of the high-P metamorphic rocks through the subduction zone. The combination of ongoing subduction, thrust-assisted exhumation, and buttress effect provided a kinematic frame in which the Variscan high-P metamorphic rocks (including the Llera thrust) were bent into large recumbent folds upon synthetic and antithetic shearing to subduction polarity. Such folding and shearing drove the underplating of the high-P metamorphic rocks, which became a relaminant under the upper plate (Figure 12h).

Relamination is a poorly documented process in natural cases, perhaps due to the intrinsic complexity of the structure that derives from it. We suggest that the sequence of major structures observed in our study case, namely lithospheric thrusting and then large-scale recumbent folding, are inherent to relamination. On the one hand, deep-seated rocks in a subduction zone require major thrusts to reach the upper plate. On the other hand, partly exhumed high-P metamorphic rocks derived from a subduction zone would show a primary or secondary fabric near-parallel to the major structure(s) that controlled their exhumation (e.g., large-scale thrusts). Except for the case of flat-subduction, there will be an angle between the base of the crust's upper plate and the subduction zone. Accordingly, any shearing related to relamination (subhorizontal flow under the upper plate) would likely be oblique to previous structures developed on the partly exhumed high-P metamorphic rocks, an ideal situation for either simple shear and/or pure shear folding at a large scale.

Data Availability Statement

The structural data used for analysis in this study are available at Mendeley Data via https://doi.org/10.17632/83ffn959js.1 with CC BY 4.0 license (Díez Fernández, 2024).

Acknowledgments
This publication is part of project PID2020-112489GB-C22, funded by MCIN/AEI/https://doi.org/10.13039/501100011033. This manuscript benefited from fruitful discussions with Drs. Carlos Fernández and Luis González Menéndez, and from comments posed by four reviewers.

References

Abalos, B. (1989). Structural geology of the Ribera del Fresno window (Badajoz, Badajoz-Córdoba Shear Zone). *Revista de la Sociedad Geologica de Espana*, *2*(1–2), 103–112.

Abalos, B. (1990). *Cinemática y mecanismos de la deformación en régimen de transpresión. Evolución estructural y metamórfica de la Zona de Cizalla Dúctil de Badajoz-Córdoba* (PhD thesis) (p. 430). Universidad del País Vasco.

Abalos, B. (1992). Variscan shear-zone deformation of late Precambrian basement in SW Iberia: Implications for circum-Atlantic pre-Mesozoic tectonics. *Journal of Structural Geology*, *14*(7), 807–823. https://doi.org/10.1016/0191-8141(92)90042-u

Abalos, B., & Eguiluz, L. (1991). Deformación transpresiva carbonífera en la Zona de Cizalla de Badajoz-Córdoba (Macizo Ibérico meridional). *Revista de la Sociedad Geologica de Espana*, *4*(3–4), 229–249.

Abalos, B., Eguiluz, L., & Gil Ibarguchi, J. I. (1991a). Evolución tectono-metamórfica del Corredor Blastomilonítico de Badajoz-Córdoba. I: La Unidad Para-Autóctona. *Boletin Geologico y Minero*, *102–4*, 491–523.

Abalos, B., Eguiluz, L., & Gil Ibarguchi, J. I. (1991b). Evolución tectono-metamórfica del Corredor Blastomilonítico de Badajoz-Córdoba. II: Las unidades alóctonas y trayectorias PTt. *Boletin Geologico y Minero*, *102–5*, 617–671.

Abalos, B., Gil Ibarguchi, J. I., & Eguiluz, L. (1991c). Cadomian subduction, collision and Variscan transpression in the Badajoz-Cordoba shear belt, southwest Spain. *Tectonophysics*, *199*(1), 51–72. https://doi.org/10.1016/0040-1951(91)90118-c

Ábalos, B., Puelles, P., & Gil Ibarguchi, J. I. (2023). Polyphase tectonic reworking of serpentinites and chlorite-tremolite-talc rocks (SW Spain) from the subduction forearc to intracontinental emplacement. *Journal of Metamorphic Geology*, *41*(4), 491–523. https://doi.org/10.1111/jmg.12704

Abati, J., Arenas, R., Díez Fernández, R., Albert, R., & Gerdes, A. (2018). Combined zircon U-Pb and Lu-Hf isotopes study of magmatism and high-P metamorphism of the basal allochthonous units in the SW Iberian Massif (Ossa-Morena complex). *Lithos*, *322*, 20–37. https://doi.org/10.1016/j.lithos.2018.07.032

Andersen, T. B., Jamtveit, B., Dewey, J. F., & Swensson, E. (1991). Subduction and eduction of continental-crust - major mechanisms during continent-continent collision and orogenic extensional collapse, a model based on the South Norwegian Caledonides. *Terra Nova*, *3*, 303–310. https://doi.org/10.1111/j.1365-3121.1991.tb00148.x

Apalategui, O., Eguiluz, L., & Quesada, C. (1990). Ossa-Morena zone: Structure. In R. D. Dallmeyer & E. Martínez García (Eds.), *Pre-mesozoic geology of Iberia* (pp. 280–292). Springer-Verlag.

Arango, C., Díez Fernández, R., & Arenas, R. (2013). Large-scale flat-lying isoclinal folding in extending lithosphere: Santa María de la Alameda dome (Central Iberian Massif, Spain). *Lithosphere*, *5*, 483–500. https://doi.org/10.1130/L270.1

Arenas, R., Fernández-Suárez, J., Montero, P., Díez Fernández, R., Andonaegui, P., Sánchez Martínez, S., et al. (2018). The Calzadilla Ophiolite (SW Iberia) and the Ediacaran fore-arc evolution of the African margin of Gondwana. *Gondwana Research*, *58*, 71–86. https://doi.org/10.1016/j.gr.2018.01.015

Arenas, R., Novo-Fernández, I., Garcia-Casco, A., Díez Fernández, R., Fuenlabrada, J. M., Pereira, M. F., et al. (2021). A unique blueschist facies metapelite with Mg-rich chloritoid from the Badajoz-Córdoba Unit (SW Iberian Massif): Correlation of late Devonian high-pressure belts along the Variscan Orogen. *International Geology Review*, *63*(13), 1634–1657. https://doi.org/10.1080/00206814.2020.1789509

Armendariz, M., López-Guijarro, R., Quesada, C., Pin, C., & Bellido, F. (2008). Genesis and evolution of a syn-orogenic basin in transpression: Insights from petrography, geochemistry and Sm-Nd systematics in the Variscan Pedroches basin (Mississippian, SW Iberia). *Tectonophysics*, *461*(1–4), 395–413. https://doi.org/10.1016/j.tecto.2008.02.007

Azor, A. (1994). *Evolución tectonometamórfica del límite entre las zonas Centroibérica y de Ossa-Morena (Cordillera Varisca, SO de España)* (p. 312). Universidad de Granada.

Azor, A., Lodeiro, F. G., & Simancas, J. F. (1994). Tectonic evolution of the boundary between the Central Iberian and Ossa-Morena zones (Variscan belt, southwest Spain). *Tectonics*, *13*(1), 45–61. https://doi.org/10.1029/93tc02724

Bea, F., Montero, P., Haissen, F., Molina, J. F., Michard, A., Lazaro, C., et al. (2016). First evidence for Cambrian rift-related magmatism in the West African Craton margin: The Derraman Peralkaline felsic complex. *Gondwana Research*, *36*, 423–438. https://doi.org/10.1016/j.gr.2015.07.017

Beaumont, C., Jamieson, R. A., Butler, J. P., & Warren, C. J. (2009). Crustal structure: A key constraint on the mechanism of ultra-high-pressure rock exhumation. *Earth and Planetary Science Letters*, *287*(1–2), 116–129. https://doi.org/10.1016/j.epsl.2009.08.001

Blatrix, P., & Burg, J. P. (1981). 40Ar/39Ar dates from Sierra Morena (southern Spain): Variscan metamorphism and Cadomian orogeny. *Neues Jahrbuch für Mineralogie - Monatshefte*, *10*, 470–478.

Borg, I., & Handin, J. (1966). Experimental deformation of crystalline rocks. *Tectonophysics*, *3*(4), 249–367. https://doi.org/10.1016/0040-1951(66)90019-9

Bostock, M. G., Hyndman, R. D., Rondenay, S., & Peacock, S. M. (2002). An inverted continental moho and serpentinization of the forearc mantle. *Nature*, *417*(6888), 536–538. https://doi.org/10.1038/417536a

Burg, J. P., Iglesias, M., Laurent, P., Matte, P., & Ribeiro, A. (1981). Variscan intracontinental deformation: The Coimbra-Cordoba shear zone (SW Iberian Peninsula). *Tectonophysics*, *78*(1–4), 161–177. https://doi.org/10.1016/0040-1951(81)90012-3

Burov, E., Francois, T., Yamato, P., & Wolf, S. (2014). Mechanisms of continental subduction and exhumation of HP and UHP rocks. *Gondwana Research*, *25*(2), 464–493. https://doi.org/10.1016/j.gr.2012.09.010

Burov, E., Jolivet, L., Le Pourhiet, L., & Poliakov, A. (2001). A thermomechanical model of exhumation of high pressure (HP) and ultra-high pressure (UHP) metamorphic rocks in Alpine-type collision belts. *Tectonophysics*, *342*(1–2), 113–136. https://doi.org/10.1016/s0040-1951(01)00158-5

Cardozo, N., & Allmendinger, R. W. (2013). Spherical projections with OSXStereonet. *Computers & Geosciences*, *51*, 193–205. https://doi.org/10.1016/j.cageo.2012.07.021

Carter, N. L., Christie, J. M., & Griggs, D. T. (1964). Experimental deformation and recrystallization of quartz. *The Journal of Geology*, *72*(6), 687–733. https://doi.org/10.1086/627029

Castro, A., Vogt, K., & Gerya, T. (2013). Generation of new continental crust by sublithospheric silicic-magma relamination in arcs: A test of Taylor's andesite model. *Gondwana Research*, *23*(4), 1554–1566. https://doi.org/10.1016/j.gr.2012.07.004

Chacón, J. (1979). *Estudio geológico del sector central del anticlinorio Portoalegre-Badajoz-Córdoba. (Macizo Ibérico Meridional)* (PhD Thesis). (p. 728). Universidad de Granada.

Chacón, J., & Velasco, F. (1981). Rocas Ultrabásicas metamorfizadas en el Grupo de Azuaga (Anticlinorio Badajoz-Córdoba). *Cuadernos de Geologia Iberica*, *7*, 151–159.

Chemenda, A. I., Burg, J. P., & Mattauer, M. (2000). Evolutionary model of the Himalaya-Tibet system: Geopoem based on new modelling, geological and geophysical data. *Earth and Planetary Science Letters*, *174*(3–4), 397–409. https://doi.org/10.1016/s0012-821x(99)00277-0

Chemenda, A. I., Mattauer, M., Malavieille, J., & Bokun, A. N. (1995). A mechanism for syn-collisional rock exhumation and associated normal faulting - Results from physical modelling. *Earth and Planetary Science Letters*, *132*(1–4), 225–232. https://doi.org/10.1016/0012-821x(95)00042-b

Dias da Silva, Í., Pereira, M. F., Gama, C., Steel Hart, L., Barrios Sánchez, S., Alves, K. D. S., et al. (2024). The influence of synorogenic extension on the crustal architecture of north Gondwana during the assembly of Pangaea (Ossa–Morena zone, SW Iberia). *Geological Society, London, Special Publications*, *542*(1), SP542-2023-9. https://doi.org/10.1144/sp542-2023-9

Díez Fernández, R. (2024). Structural data from Devonian suture zone in SW Iberia (Central Unit, Spain) [Dataset]. *Mendeley Data, V1*. https://doi.org/10.17632/5p3563c95d.1

Díez Fernández, R., & Arenas, R. (2015). The late Devonian Variscan suture of the Iberian Massif: A correlation of high-pressure belts in NW and SW Iberia. *Tectonophysics*, *654*, 96–100. https://doi.org/10.1016/j.tecto.2015.05.001

Díez Fernández, R., & Arenas, R. (2016). Reply to comment on "The Late Devonian Variscan suture of the Iberian Massif: A correlation of high-pressure belts in NW and SW Iberia". *Tectonophysics*, *670*, 155–160. https://doi.org/10.1016/j.tecto.2015.11.033

Díez Fernández, R., Arenas, R., Pereira, M. F., Sánchez Martínez, S., Albert, R., Martín Parra, L. M., et al. (2016). Tectonic evolution of Variscan Iberia: Gondwana - Laurussia collision revisited. *Earth-Science Reviews*, *162*, 269–292. https://doi.org/10.1016/j.earscirev.2016.08.002

Díez Fernández, R., Arenas, R., Rojo-Pérez, E., Sánchez Martínez, S., & Fuenlabrada, J. M. (2022). Tectonostratigraphy of the Mérida Massif reveals a new Cadomian suture zone exposure in Gondwana (SW Iberia). *International Geology Review*, *64*(3), 405–424. https://doi.org/10.1080/00206814.2020.1858355

Díez Fernández, R., Fernández, C., Arenas, R., & Novo-Fernández, I. (2021). On the Rootless nature of a Devonian suture in SW Iberia (Ossa-Morena complex, Variscan Orogen): Geometry and kinematics of the Azuaga Fault. *Tectonics*, *40*(6), e2021TC006791. https://doi.org/10.1029/2021tc006791

Díez Fernández, R., Fernández, C., Arenas, R., & Novo-Fernández, I. (2022). Reply to Comment by Azor et al. on "On the Rootless Nature of a Devonian Suture in SW Iberia (Ossa-Morena Complex, Variscan Orogen): Geometry and Kinematics of the Azuaga Fault". *Tectonics*, *41*(1), e2021TC007154. https://doi.org/10.1029/2021tc007154

Díez Fernández, R., Foster, D. A., Gómez Barreiro, J., & Alonso-García, M. (2013). Rheological control on the tectonic evolution of a continental suture zone: The Variscan example from NW Iberia (Spain). *International Journal of Earth Sciences*, *102*(5), 1305–1319. https://doi.org/10.1007/s00531-013-0885-5

Díez Fernández, R., Jiménez-Díaz, A., Arenas, R., Pereira, M. F., & Fernández-Suárez, J. (2019). Ediacaran obduction of a fore-arc ophiolite in SW Iberia: A turning point in the evolving geodynamic setting of Peri-Gondwana. *Tectonics*, *38*(1), 95–119. https://doi.org/10.1029/2018tc005224

Díez Fernández, R., & Martínez Catalán, J. R. (2009). 3D analysis of an Ordovician igneous ensemble: A complex magmatic structure hidden in a polydeformed allochthonous Variscan unit. *Journal of Structural Geology*, *31*(3), 222–236. https://doi.org/10.1016/j.jsg.2008.11.017

Díez Fernández, R., Martínez Catalán, J. R., Arenas, R., & Abati, J. (2011). Tectonic evolution of a continental subduction-exhumation channel: Variscan structure of the basal allochthonous units in NW Spain. *Tectonics*, *30*(3), TC3009. https://doi.org/10.1029/2010tc002850

Díez Fernández, R., Martínez Catalán, J. R., Gerdes, A., Abati, J., Arenas, R., & Fernández-Suárez, J. (2010). U–Pb ages of detrital zircons from the Basal allochthonous units of NW Iberia: Provenance and paleoposition on the northern margin of Gondwana during the Neoproterozoic and Paleozoic. *Gondwana Research*, *18*(2–3), 385–399. https://doi.org/10.1016/j.gr.2009.12.006

Díez Fernández, R., Martínez Catalán, J. R., Gómez Barreiro, J., & Arenas, R. (2012). Extensional flow during gravitational collapse: A tool for setting plate convergence (Padrón migmatitic dome, Variscan belt, NW Iberia). *The Journal of Geology*, *120*(1), 83–103. https://doi.org/10.1086/662735

Díez Fernández, R., Martín Parra, L. M., & Rubio Pascual, F. J. (2017). Extensional flow produces recumbent folds in syn-orogenic granitoids (Padrón migmatitic dome, NW Iberian Massif). *Tectonophysics*, *703–704*, 69–84. https://doi.org/10.1016/j.tecto.2017.03.010

Díez Fernández, R., Matas, J., Arenas, R., Martín-Parra, L. M., Sánchez Martínez, S., Novo-Fernández, I., & Rojo-Pérez, E. (2021). Two-step obduction of the Porvenir Serpentinite: A cryptic Devonian suture in SW Iberian Massif (Ossa-Morena complex). In J. Wakabayashi & Y. Dilek (Eds.), *Plate tectonics, ophiolites, and societal significance of Geology: A celebration of the career of Eldridge Moores* (pp. 113–132). GSA Books. https://doi.org/10.1130/2021.2552(07)

Díez Fernández, R., Novo-Fernández, I., Moreno-Martín, D., Arenas, R., Rojo-Pérez, E., Martín Parra, L. M., & Matas, J. (2024). *Exhumation of high-pressure rocks: Role of late faulting (eastern Ossa-Morena complex, Iberian Massif)* (Vol. 542, pp. 527–542). Geological Society, London, Special Publications. https://doi.org/10.1144/SP542-2022-308

Díez Fernández, R., & Pereira, M. F. (2017). Strike-slip shear zones of the Iberian Massif: Are they coeval? *Lithosphere*, *9*(5), 726–744. https://doi.org/10.1130/l648.1

Díez Montes, A., Martínez Catalán, J. R., & Bellido Mulas, F. (2010). Role of the Ollo de Sapo massive felsic volcanism of NW Iberia in the Early Ordovician dynamics of northern Gondwana. *Gondwana Research*, *17*(2–3), 363–376. https://doi.org/10.1016/j.gr.2009.09.001

Duretz, T., Gerya, T. V., Kaus, B. J. P., & Andersen, T. B. (2012). Thermomechanical modeling of slab eduction. *Journal of Geophysical Research: Solid Earth*, *117*(B8). https://doi.org/10.1029/2012jb009137

Eguíluz, L. (1987). *Petrogénesis de rocas ígneas y metamórficas en el Antiforme Burguillos-Monesterio, Macizo Ibérico Meridional* (Ph.D. Thesis). (p. 694). Universidad del País Vasco.

Eguíluz, L., Gil Ibarguchi, J. I., Abalos, B., & Apraiz, A. (2000). Superposed Hercynian and Cadomian orogenic cycles in the Ossa-Morena zone and related areas of the Iberian Massif. *Geological Society of America Bulletin*, *112*(9), 1398–1413. https://doi.org/10.1130/0016-7606(2000)112<1398:shacoc>2.0.co;2

Expósito, I., Simancas, J. F., González Lodeiro, F., Azor, A., & Martínez Poyatos, D. J. (2002). La estructura de la mitad septentrional de la Zona de Ossa-Morena: Deformación en el bloque inferior de un cabalgamiento cortical de evolución compleja. *Revista de la Sociedad Geologica de Espana*, *15*, 3–14.

Expósito, I., Simancas, J. F., González Lodeiro, F., Bea, F., Montero, P., & Salman, K. (2003). Metamorphic and deformational imprint of Cambrian-lower Ordovician rifting in the Ossa-Morena zone (Iberian Massif, Spain). *Journal of Structural Geology*, *25*(12), 2077–2087. https://doi.org/10.1016/s0191-8141(03)00075-0

Faure, M., Bé Mézème, E., Cocherie, A., Rossi, P., Chemenda, A., & Boutelier, D. (2008). Devonian geodynamic evolution of the Variscan belt, insights from the French Massif central and Massif Armoricain. *Tectonics*, *27*(2), TC2005. https://doi.org/10.1029/2007tc002115

Faure, M., Lin, W., Schärer, U., Shu, L., Sun, Y., & Arnaud, N. (2003). Continental subduction and exhumation of UHP rocks. Structural and geochronological insights from the Dabieshan (East China). *Lithos*, *70*(3–4), 213–241. https://doi.org/10.1016/s0024-4937(03)00100-2

Faure, M., Marcoux, E., Poujol, M., & Masson, C. (2025). How Stiff was Armorica during the Variscan Orogeny? A reappraisal of the "Bretonian" phase in central Brittany. *Geosciences*, *15*(2), 60. https://doi.org/10.3390/geosciences15020060

Fossen, H., & Cavalcante, G. C. G. (2017). Shear zones – A review. *Earth-Science Reviews*, *171*, 434–455. https://doi.org/10.1016/j.earscirev.2017.05.002

Franek, J., Schulmann, K., Lexa, O., Tomek, Č., & Edel, J.-B. (2011). Model of syn-convergent extrusion of orogenic lower crust in the core of the Variscan belt: Implications for exhumation of high-pressure rocks in large hot orogens. *Journal of Metamorphic Geology*, *29*(1), 53–78. https://doi.org/10.1111/j.1525-1314.2010.00903.x

Franke, W., & Stein, E. (2000). Exhumation of high-grade rocks in the Saxo-Thuringian Belt: Geological constraints and geodynamic concepts. *Geological Society, London, Special Publications*, *179*(1), 337–354. https://doi.org/10.1144/gsl.sp.2000.179.01.20

Fuenlabrada, J. M., Arenas, R., Díez Fernández, R., González del Tánago, J., Martín-Parra, L. M., Matas, J., et al. (2021). Tectonic setting and isotopic sources (Sm–Nd) of the SW Iberian autochthon (Variscan Orogen). *Journal of Iberian Geology*, *47*(1–2), 121–150. https://doi.org/10.1007/s41513-020-00148-7

Furlong, K. P., & Fountain, D. M. (1986). Continental crustal underplating: Thermal considerations and seismic-petrologic consequences. *Journal of Geophysical Research: Solid Earth*, *91*(B8), 8285–8294. https://doi.org/10.1029/jb091ib08p08285

García Casquero, J. L., Priem, H. N. A., Boelrijk, N. A. I. M., & Chacon, J. (1988). Isotopic dating of the mylonitization of the Azuaga group in the Badajóz-Córdoba belt, SW Spain. *Geologische Rundschau*, *77*(2), 483–489. https://doi.org/10.1007/bf01832393

Gerya, T. (2022). Numerical modeling of subduction: State of the art and future directions. *Geosphere*, *18*(2), 503–561. https://doi.org/10.1130/ges02416.1

Gerya, T. V., Perchuk, L. L., & Burg, J.-P. (2008). Transient hot channels: Perpetrating and regurgitating ultrahigh-pressure, high-temperature crust–mantle associations in collision belts. *Lithos*, *103*(1–2), 236–256. https://doi.org/10.1016/j.lithos.2007.09.017

Gerya, T. V., Stöckhert, B., & Perchuk, A. (2002). Exhumation of high-pressure metamorphic rocks in a subduction channel: A numerical simulation. *Tectonics*, *21*(6), 1056. https://doi.org/10.1029/2002tc001406

Gómez-Pugnaire, M. T., Azor, A., Fernández-Soler, J. M., & Sánchez-Vizcaíno, V. L. (2003). The amphibolites from the Ossa–Morena/Central Iberian Variscan suture (Southwestern Iberian Massif): Geochemistry and tectonic interpretation. *Lithos*, *68*(1–2), 23–42. https://doi.org/10.1016/s0024-4937(03)00018-5

Gottschalk, R. R., Kronenberg, A. K., Russell, J. E., & Handin, J. (1990). Mechanical anisotropy of gneiss: Failure criterion and textural sources of directional behavior. *Journal of Geophysical Research*, *95*(B13), 21613–21634. https://doi.org/10.1029/jb095ib13p21613

Grujic, D., Warren, C. J., & Wooden, J. L. (2011). Rapid synconvergent exhumation of Miocene-aged lower orogenic crust in the eastern Himalaya. *Lithosphere*, *3*(5), 346–366. https://doi.org/10.1130/l154.1

Guillot, S., Hattori, K., Agard, P., Schwartz, S., & Vidal, O. (2009). Exhumation processes in oceanic and continental subduction contexts: A review. In S. Lallemand & F. Funiciello (Eds.), *Subduction zone geodynamics* (pp. 175–205). Frontiers in Earth Sciences.

Guilmette, C., Indares, A., & Hébert, R. (2011). High-pressure anatectic paragneisses from the Namche Barwa, Eastern Himalayan Syntaxis: Textural evidence for partial melting, phase equilibria modeling and tectonic implications. *Lithos*, *124*(1), 66–81. https://doi.org/10.1016/j.lithos.2010.09.003

Hacker, B. R., Gerya, T. V., & Gilotti, J. A. (2013). Formation and exhumation of ultrahigh-pressure terranes. *Elements*, *9*(4), 289–293. https://doi.org/10.2113/gselements.9.4.289

Hacker, B. R., Kelemen, P. B., & Behn, M. D. (2011). Differentiation of the continental crust by relamination. *Earth and Planetary Science Letters*, *307*(3), 501–516. https://doi.org/10.1016/j.epsl.2011.05.024

Hyndman, R. D., & Peacock, S. M. (2003). Serpentinization of the forearc mantle. *Earth and Planetary Science Letters*, *212*(3), 417–432. https://doi.org/10.1016/s0012-821x(03)00263-2

Johnston, S. M., Hacker, B. R., & Andersen, T. B. (2007). Exhuming Norwegian ultrahigh-pressure rocks: Overprinting extensional structures and the role of the Nordfjord-Sogn Detachment Zone. *Tectonics*, *26*(5). https://doi.org/10.1029/2005tc001933

Jolivet, L., & Brun, J.-P. (2010). Cenozoic geodynamic evolution of the Aegean. *International Journal of Earth Sciences*, *99*(1), 109–138. https://doi.org/10.1007/s00531-008-0366-4

Jolivet, L., Faccenna, C., Goffé, B., Burov, E., & Agard, P. (2003). Subduction tectonics and exhumation of high-pressure metamorphic rocks in the Mediterranean orogens. *American Journal of Science*, *303*(5), 353–409. https://doi.org/10.2475/ajs.303.5.353

Kali, E., Leloup, P. H., Arnaud, N., Mahéo, G., Liu, D., Boutonnet, E., et al. (2010). Exhumation history of the deepest central Himalayan rocks, Ama Drime range: Key pressure-temperature-deformation-time constraints on orogenic models. *Tectonics*, *29*(2). https://doi.org/10.1029/2009tc002551

Kellett, D. A., Grujic, D., Warren, C., Cottle, J., Jamieson, R., & Tenzin, T. (2010). Metamorphic history of a syn-convergent orogen-parallel detachment: The South Tibetan detachment system, Bhutan Himalaya. *Journal of Metamorphic Geology*, *28*(8), 785–808. https://doi.org/10.1111/j.1525-1314.2010.00893.x

Konopasek, J., & Schulmann, K. (2005). Contrasting early carboniferous field geotherms: Evidence for accretion of a thickened orogenic root and subducted Saxothuringian crust (central European Variscides). *Journal of the Geological Society*, *162*(3), 463–470. https://doi.org/10.1144/0016-764904-004

Kroner, U., & Romer, R. L. (2013). Two plates—Many subduction zones: The Variscan Orogeny reconsidered. *Gondwana Research*, *24*(1), 298–329. https://doi.org/10.1016/j.gr.2013.03.001

Linnemann, U., Gerdes, A., Drost, K., & Buschmann, B. (2007). The continuum between Cadomian orogenesis and opening of the Rheic Ocean: Constraints from LA-ICP-MS U–Pb zircon dating and analysis of plate-tectonic setting (Saxo-Thuringian zone, northeastern Bohemian Massif, Germany). In U. Linnemann, R. D. Nance, P. Kraft, & G. Zulauf (Eds.), *The evolution of the Rheic Ocean: From Avalonian-Cadomian active margin to Alleghenian-Variscan collision* (pp. 61–96). Geological Society of America Special Paper. https://doi.org/10.1130/2007.2423(03

Linnemann, U., Gerdes, A., Hofmann, M., & Marko, L. (2014). The Cadomian orogen: Neoproterozoic to early Cambrian crustal growth and orogenic zoning along the periphery of the West African Craton—Constraints from U–Pb zircon ages and Hf isotopes (Schwarzburg antiform, Germany). *Precambrian Research*, *244*, 236–278. https://doi.org/10.1016/j.precamres.2013.08.007

Little, T. A., Hacker, B. R., Gordon, S. M., Baldwin, S. L., Fitzgerald, P. G., Ellis, S., & Korchinski, M. (2011). Diapiric exhumation of Earth's youngest (UHP) eclogites in the gneiss domes of the D'Entrecasteaux Islands, Papua New Guinea. *Tectonophysics*, *510*(1), 39–68. https://doi.org/10.1016/j.tecto.2011.06.006

López Sánchez-Vizcaíno, V., Gómez-Pugnaire, M. T., Azor, A., & Fernández-Soler, J. M. (2003). Phase diagram sections applied to amphibolites: A case study from the Ossa-Morena/central Iberian Variscan suture (Southwestern Iberian Massif). *Lithos*, *68*(1), 1–21. https://doi.org/10.1016/s0024-4937(03)00017-3

Moreno-Martín, D., Díez Fernández, R., Arenas, R., Rojo-Pérez, E., Novo-Fernández, I., & Sánchez Martínez, S. (2023). Building and collapse of the Cadomian orogen: A plate-scale model based on structural data from the SW Iberian Massif. *Tectonics*, *42*(12), e2023TC007990. https://doi.org/10.1029/2023tc007990

Magni, V., Allen, M. B., van Hunen, J., & Bouilhol, P. (2017). Continental underplating after slab break-off. *Earth and Planetary Science Letters*, *474*, 59–67. https://doi.org/10.1016/j.epsl.2017.06.017

Maierová, P., Schulmann, K., & Gerya, T. (2018). Relamination styles in collisional orogens. *Tectonics*, *37*(1), 224–250. https://doi.org/10.1002/2017tc004677

Martin, C., Flores, K. E., Vitale-Brovarone, A., Angiboust, S., & Harlow, G. E. (2020). Deep mantle serpentinization in subduction zones: Insight from in situ B isotopes in slab and mantle wedge serpentinites. *Chemical Geology*, *545*, 119637. https://doi.org/10.1016/j.chemgeo.2020.119637

Martínez Catalán, J. R. (2011). Are the oroclines of the Variscan belt related to late Variscan strike-slip tectonics? *Terra Nova*, *23*(4), 241–247. https://doi.org/10.1111/j.1365-3121.2011.01005.x

Martínez Catalán, J. R., Collett, S., Schulmann, K., Aleksandrowski, P., & Mazur, S. (2020). Correlation of allochthonous terranes and major tectonostratigraphic domains between NW Iberia and the Bohemian Massif, European Variscan belt. *International Journal of Earth Sciences*, *109*(4), 1105–1131. https://doi.org/10.1007/s00531-019-01800-z

Martínez Catalán, J. R., Rubio Pascual, F. J., Díez Montes, A., Díez Fernández, R., Gómez Barreiro, J., Dias da Silva, Í., et al. (2014). The late Variscan HT/LP metamorphic event in NW and central Iberia: Relationships to crustal thickening, extension, orocline development and crustal evolution. In K. Schulmann, J. R. Martínez Catalán, J. M. Lardeaux, V. Janoušek, & G. Oggiano (Eds.), *The Variscan Orogeny: Extent, timescale and the formation of the European crust* (pp. 225–247). Geological Society of London Special Publication. https://doi.org/10.1144/SP405.1

Martínez Catalán, J. R., Schulmann, K., & Ghienne, J.-F. (2021). The Mid-Variscan Allochthon: Keys from correlation, partial retrodeformation and plate-tectonic reconstruction to unlock the geometry of a non-cylindrical belt. *Earth-Science Reviews*, *220*, 103700. https://doi.org/10.1016/j.earscirev.2021.103700

Martínez Poyatos, D., González Lodeiro, F., Azor, A., & Simancas, J. F. (2001). La estructura de la Zona Centroibérica en la región de Los Pedroches (Macizo Ibérico meridional). *Revista de la Sociedad Geologica de Espana*, *14*, 147–160.

Martínez Poyatos, D., Simancas, J. F., Azor, A., & González Lodeiro, F. (1995). La estructura del borde meridional de la Zona Centroibérica en el sector suroriental de la Provincia de Badajoz. *Revista de la Sociedad Geologica de Espana*, *8*, 41–50.

Martínez Poyatos, D., Simancas, J. F., Azor, A., & González Lodeiro, F. (1998). Evolution of a Carboniferous piggyback basin in the southern central Iberian zone (Variscan belt, SE Spain). *Bulletin de la Societe Geologique de France*, *169*, 573–578.

Martínez Poyatos, D. J. (2002). Estructura del borde meridional de la Zona Centroibérica y su relación con el contacto entre las Zonas Centroibérica y de Ossa-Morena. *Nova Terra*, *18*, 1–295.

Matas, J., Martín Parra, L., & Montes Santiago, M. (2014). Un olistostroma con cantos y bloques del Paleozoico Inferior en la cuenca carbonífera del Guadalmellato (Córdoba). Parte I: Estratigrafía y marco geodinámico varisco. *Revista de la Sociedad Geologica de Espana*, *27*(1), 11–26.

Matas, J., Martín Parra, L. M., & Martínez Poyatos, D. (2015). *Mapa y Memoria del Mapa Geológico Nacional a escala 1:200.000 (MAGE200) nº 69 (Pozoblanco)*. Instituto Geológico y Minero de España.

Matas, J., Martín Parra, L. M., Roldán, F. J., & Martín-Serrano, A. (2015). *Mapa y Memoria del Mapa Geológico Nacional a escala 1:200.000 (MAGE200) nº 76 (Córdoba)*. Instituto Geológico y Minero de España.

Matte, P. (2001). The Variscan collage and orogeny (480-290 Ma) and the tectonic definition of the Armorica microplate: A review. *Terra Nova*, *13*(2), 122–128. https://doi.org/10.1046/j.1365-3121.2001.00327.x

Moreno-Martín, D., Díez Fernández, R., Albert, R., Sánchez Martínez, S., Rojo-Pérez, E., Gerdes, A., & Arenas, R. (2025). Cuartel Ophiolite: Structure, timing and exhumation mechanisms for a Cadomian suture zone in the peri-Gondwanan Realm (SW Iberia). *Gondwana Research*, *137*, 255–273. https://doi.org/10.1016/j.gr.2024.10.002

Nance, R. D., & Murphy, J. B. (1994). Contrasting basement isotopic signatures and the palinspastic restoration of peripheral orogens: Example from the Neoproterozoic Avalonian-Cadomian belt. *Geology*, *22*(7), 617–620. https://doi.org/10.1130/0091-7613(1994)022<0617:cbisat>2.3.co;2

Nance, R. D., Murphy, J. B., Strachan, R. A., Keppie, J. D., Gutiérrez-Alonso, G., Fernández-Suárez, J., et al. (2008). Neoproterozoic-early Palaeozoic tectonostratigraphy and palaeogeography of the peri-Gondwanan terranes: Amazonian v. West African connections. In N. Ennih & J. P. Liégeois (Eds.), *The boundaries of the West African Craton* (pp. 345–383). Geological Society, London, Special Publications. https://doi.org/10.1144/SP297.17

Novo-Fernández, I., Arenas, R., de Capitani, C., Pereira, M. F., Díez Fernández, R., Sánchez Martínez, S., & Garcia-Casco, A. (2021). Tracking the late Devonian high-P metamorphic belt in the Variscan orogen: New constraints on the PT evolution of eclogites from the Cubito-Moura Unit (SW Iberian Massif). *Lithos*, *386–387*, 106015. https://doi.org/10.1016/j.lithos.2021.106015

Ordóñez Casado, B. (1998). *Geochronological studies of the pre-Mesozoic basement of the Iberian Massif: The Ossa Morena zone and the Allochthonous Complexes within the central Iberian zone* (PhD Thesis). (p. 235). Swiss Federal Institute of Technology.

Ouabid, M., Ouali, H., Garrido, C. J., Acosta-Vigil, A., Román-Alpiste, M. J., Dautria, J.-M., et al. (2017). Neoproterozoic granitoids in the basement of the Moroccan central Meseta: Correlation with the anti-Atlas at the NW paleo-margin of Gondwana. *Precambrian Research*, *299*, 34–57. https://doi.org/10.1016/j.precamres.2017.07.007

Pereira, M. F. (1999). *Caracterização da estrutura dos domínios setentrionais da zona de Ossa-Morena e seu limite com a zona centro-ibérica, no nordeste alentejano* (PhD thesis, p. 114). Universidade de Évora.

Pereira, M. F., Apraiz, A., Chichorro, M., Silva, J. B., & Armstrong, R. A. (2010). Exhumation of high-pressure rocks in northern Gondwana during the Early Carboniferours (Coimbra-Cordoba shear zone, SW Iberian Massif): Tectonothermal analysis and U–Th–Pb SHRIMP in-situ zircon geochronology. *Gondwana Research*, *17*(2–3), 440–460. https://doi.org/10.1016/j.gr.2009.10.001

Pereira, M. F., Chichorro, M., Williams, I. S., Silva, J. B., Fernández, C., Díaz-Azpíroz, M., et al. (2009). Variscan intra-orogenic extensional tectonics in the Ossa-Morena Zone (Évora-Aracena-Lora del Río metamorphic belt, SW Iberian Massif): SHRIMP zircon U–Th–Pb geochronology. *Geological Society, London, Special Publications*, *327*(1), 215–237. https://doi.org/10.1144/sp327.11

Pereira, M. F., Silva, J. B., Drost, K., Chichorro, M., & Apraiz, A. (2010). Relative timing of transcurrent displacements in northern Gondwana: U–Pb laser ablation ICP-MS zircon and monazite geochronology of gneisses and sheared granites from the western Iberian Massif (Portugal). *Gondwana Research*, *17*(2–3), 461–481. https://doi.org/10.1016/j.gr.2009.08.006

Pérez-Cáceres, I., Simancas, J. F., Martínez Poyatos, D., Azor, A., & González Lodeiro, F. (2016). Oblique collision and deformation partitioning in the SW Iberian Variscides. *Solid Earth*, *7*(3), 857–872. https://doi.org/10.5194/se-7-857-2016

Platt, J. P. (1993). Exhumation of high-pressure rocks: A review of concepts and processes. *Terra Nova*, *5*(2), 119–133. https://doi.org/10.1111/j.1365-3121.1993.tb00237.x

Quesada, C. (1990). Precambrian successions in SW Iberia: Their relationship to 'Cadomian' orogenic events. In D. R. Lemos, R. A. Strachan, & C. G. Topley (Eds.), *The Cadomian orogeny* (pp. 353–362). Geological Society, London, Special Publication. Geological Society, London, Special Publication.

Quesada, C., & Dallmeyer, R. D. (1994). Tectonothermal evolution of the Badajoz-Cordoba shear zone (SW Iberia): Characteristics and $^{40}Ar/^{39}Ar$ mineral age constraints. *Tectonophysics*, *231*(1–3), 195–213. https://doi.org/10.1016/0040-1951(94)90130-9

Rojo-Pérez, E., Fuenlabrada, J. M., Díez Fernández, R., & Arenas, R. (2024). Origin and evolution of Cadomian magmatism in SW Iberia: From subduction onset and arc building to a tectonic switching. *International Geology Review*, *66*(10), 1885–1909. https://doi.org/10.1080/00206814.2023.2258394

Rojo-Pérez, E., Linnemann, U., Hofmann, M., Fuenlabrada, J. M., Zieger, J., Fernández-Suárez, J., et al. (2022). U-Pb geochronology and isotopic geochemistry of adakites and related magmas in the Ediacaran arc section of the SW Iberian Massif: The role of subduction erosion cycles in peri-Gondwanan arcs. *Gondwana Research*, *109*, 89–112. https://doi.org/10.1016/j.gr.2022.04.011

Rubio Pascual, F. J., Arenas, R., Catalán, J. R. M., Fernández, L. R. R., & Wijbrans, J. R. (2013). Thickening and exhumation of the Variscan roots in the Iberian central system: Tectonothermal processes and 40Ar/39Ar ages. *Tectonophysics*, *587*, 207–221. https://doi.org/10.1016/j.tecto.2012.10.005

Rubio Pascual, F. J., Martín Parra, L. M., Díez Fernández, R., Valverde-Vaquero, P., Díez-Montes, A., Hacar Rodríguez, M. P., et al. (2024). Tectonics and geothermal gradients from subduction to collision in the NW Variscan Iberian Massif. *International Geology Review*, *66*(1), 380–404. https://doi.org/10.1080/00206814.2022.2073569

Sánchez-Lorda, M. E., Ábalos, B., García de Madinabeitia, S., Eguíluz, L., Gil Ibarguchi, J. I., & Paquette, J. L. (2016). Radiometric discrimination of pre-Variscan amphibolites in the Ediacaran serie Negra (Ossa-Morena zone, SW Iberia). *Tectonophysics*, *681*, 31–45. https://doi.org/10.1016/j.tecto.2015.09.020

Sang, M., Tan, Z., Xiao, W., Mao, Q., Wang, H., Li, R., & Qiao, Q. (2023). Formation of the eclogites of the Atbashi complex, Kyrgyzstan, in a subduction zone mélange diapir. *Communications Earth & Environment*, *4*(1), 434. https://doi.org/10.1038/s43247-023-01106-8

Sarrionandia, F., Errandonea-Martin, J., Larrondo, E., Carracedo-Sánchez, M., Ábalos, B., & Gil Ibarguchi, J. I. (2023). Low–Ti continental Tholeiite Origin of magmas with Calc-alkaline Signature in transcurrent settings: The Mississippian Matachel volcanic field (SW Iberian Massif). *Geochemistry, Geophysics, Geosystems*, *24*(11), e2023GC011139. https://doi.org/10.1029/2023gc011139

Schulmann, K., Lexa, O., Janoušek, V., Lardeaux, J. M., & Edel, J. B. (2014). Anatomy of a diffuse cryptic suture zone: An example from the Bohemian Massif, European Variscides. *Geology*, *42*(4), 275–278. https://doi.org/10.1130/g35290.1

Shea, W. T., & Kronenberg, A. K. (1992). Rheology and deformation mechanisms of an Isotropic mica schist. *Journal of Geophysical Research*, *97*(B11), 15201–15237. https://doi.org/10.1029/92jb00620

Shea, W. T., & Kronenberg, A. K. (1993). Strength and anisotropy of foliated rocks with varied mica contents. *Journal of Structural Geology*, *15*(9–10), 1097–1121. https://doi.org/10.1016/0191-8141(93)90158-7

Simancas, F., Expósito, I., Azor, A., Martínez Poyatos, D., & González Lodeiro, F. (2004). From the Cadomian orogenesis to the early Palaeozoic Variscan rifting in southwest Iberia. *Journal of Iberian Geology*, *30*, 53–71.

Simancas, J. F., Azor, A., Martínez-Poyatos, D., Tahiri, A., El Hadi, H., González-Lodeiro, F., et al. (2009). Tectonic relationships of southwest Iberia with the allochthons of Northwest Iberia and the Moroccan Variscides. *Comptes Rendus Geoscience*, *341*(2–3), 103–113. https://doi.org/10.1016/j.crte.2008.11.003

Sizova, E., Gerya, T., & Brown, M. (2012). Exhumation mechanisms of melt-bearing ultrahigh pressure crustal rocks during collision of spontaneously moving plates. *Journal of Metamorphic Geology*, *30*(9), 927–955. https://doi.org/10.1111/j.1525-1314.2012.01004.x

Solá, A. R., Williams, I. S., Neiva, A. M. R., & Ribeiro, M. L. (2009). U–Th–Pb SHRIMP ages and oxygen isotope composition of zircon from two contrasting late Variscan granitoids, Nisa-Albuquerque batholith, SW Iberian Massif: Petrologic and regional implications. *Lithos*, *111*(3–4), 156–167. https://doi.org/10.1016/j.lithos.2009.03.045

Solís-Alulima, B., Abati, J., López-Carmona, A., Gutiérrez-Alonso, G., Fernández-Suárez, J., & Stockli, D. F. (2022). Detrital zircon ages and provenance of a Cambrian succession in the Sierra Albarrana domain (SW Iberian Massif). *Lithos*, *408–409*, 106542. https://doi.org/10.1016/j.lithos.2021.106542

Solís-Alulima, B., López-Carmona, A., Abati, J., Rojas-Agramonte, Y., Bousquet, R., & del Tánago, J. G. (2023). Polycyclic metamorphic evolution of the Sierra Albarrana schists (SW Iberian Massif): From low-pressure Ordovician rifting to medium-pressure Variscan overprint. *Lithos*, *444–445*, 107092. https://doi.org/10.1016/j.lithos.2023.107092

Stephan, T., Kroner, U. W. E., & Romer, R. L. (2019). The pre-orogenic detrital zircon record of the Peri-Gondwanan crust. *Geological Magazine*, *156*(2), 281–307. https://doi.org/10.1017/s0016756818000031

Tirel, C., Brun, J.-P., Burov, E., Wortel, M. J. R., & Lebedev, S. (2013). A plate tectonics oddity: Caterpillar-walk exhumation of subducted continental crust. *Geology*, *41*(5), 555–558. https://doi.org/10.1130/g33862.1

Vanderhaeghe, O. (2012). The thermal-mechanical evolution of crustal orogenic belts at convergent plate boundaries: A reappraisal of the orogenic cycle. *Journal of Geodynamics*, *56–57*, 124–145. https://doi.org/10.1016/j.jog.2011.10.004

Vanderhaeghe, O., Laurent, O., Gardien, V., Moyen, J.-F., Gébelin, A., Chelle-Michou, C., et al. (2020). Flow of partially molten crust controlling construction, growth and collapse of the Variscan orogenic belt: The geologic record of the French Massif central. *BSGF - Earth Sciences Bulletin*, *191*, 25. https://doi.org/10.1051/bsgf/2020013

Vermeesch, P. (2018). IsoplotR: A free and open toolbox for geochronology. *Geoscience Frontiers*, *9*(5), 1479–1493. https://doi.org/10.1016/j.gsf.2018.04.001

Wagner, R. H. (2004). The Iberian Massif: A Carboniferous assembly. *Journal of Iberian Geology*, *30*, 93–108.

Wakabayashi, J. (2015). Anatomy of a subduction complex: Architecture of the Franciscan complex, California, at multiple length and time scales. *International Geology Review*, *57*(5–8), 669–746. https://doi.org/10.1080/00206814.2014.998728

Warren, C. J. (2013). Exhumation of (ultra-)high-pressure terranes: Concepts and mechanisms. *Solid Earth*, *4*(1), 75–92. https://doi.org/10.5194/se-4-75-2013

Warren, C. J., Beaumont, C., & Jamieson, R. A. (2008). Modelling tectonic styles and ultra-high pressure (UHP) rock exhumation during the transition from oceanic subduction to continental collision. *Earth and Planetary Science Letters*, *267*(1–2), 129–145. https://doi.org/10.1016/j.epsl.2007.11.025

Warren, C. J., Grujic, D., Kellett, D. A., Cottle, J., Jamieson, R. A., & Ghalley, K. S. (2011). Probing the depths of the India-Asia collision: U-Th-Pb monazite chronology of granulites from NW Bhutan. *Tectonics*, *30*(2). https://doi.org/10.1029/2010tc002738

Zhou, G., Zhang, J., Mattinson, C. G., Lu, Z., Mao, X., & Teng, X. (2022). Exhumation of deeply subducted continental crust along contrasting pathways: Examples from the North Qaidam ultrahigh pressure metamorphic terrane, North Tibet. *Gondwana Research*, *103*, 221–242. https://doi.org/10.1016/j.gr.2021.11.015

References From the Supporting Information

Wiedenbeck, M., Hanchar, J. M., Peck, W. H., Sylvester, P., Valley, J., Whitehouse, M., et al. (2004). Further characterisation of the 91500 Zircon Crystal. *Geostandards and Geoanalytical Research*, *28*, 9–39. https://doi.org/10.1111/j.1751-908X.2004.tb01041.x

Sláma, J., Košler, J., Condon, D. J., Crowley, J. L., Gerdes, A., Hanchar, J. M., et al. (2008). Plešovice zircon—a new natural reference material for U–Pb and Hf isotopic microanalysis. *Chemical Geology*, *249*, 1–35. https://doi.org/10.1016/j.chemgeo.2007.11.005

Paton, C., Hellstrom, J., Paul, B., Woodhead, J., & Hergt, J. (2011). Iolite: Freeware for the visualisation and processing of mass spectrometric data. *Journal of Analytical Atomic Spectrometry*, *26*, 2508–2518.